Geochemistry Geophysics Geosystems

G³

Mantle provinces under North America from multifrequency *P* wave tomography

Karin Sigloch

Department of Earth and Environmental Sciences, Ludwig-Maximilians-Universität, Theresienstrasse 41, D-80333 Munich, Germany (sigloch@geophysik.uni-muenchen.de)

[1] This is a survey of mantle provinces (large-scale seismic anomalies) under North America, from the surface down to 1500–1800 km depth. The underlying *P* velocity model was obtained by multifrequency tomography, a waveform-based method that systematically measures and models the frequency-dependence of teleseismic body waves. A novel kind of three-dimensional rendering technique is used to make the considerable structural complexities under North America accessible. In the transition zone and below, the North American mantle is dominated by seismically fast provinces, which represent distinct subduction episodes of the Farallon plate. I attempt to date and interpret the various slab fragments by reconciling their present positions with paleotrench locations from plate tectonic reconstructions and with major geologic surface episodes. Differences in vertical sinking velocity have led to large vertical offsets across adjacent, coeval slabs. Some of the mantle provinces have not been discussed much previously, including (1) a seismically slow blanket overlying the oldest Farallon subduction along the eastern continental margin, (2) a transition zone slab coeval with the Laramide orogeny (ca. 80–60 Myr), which I discuss in analogy to the "stagnant slab" subduction style commonly found in the western Pacific today, (3) the lower mantle root of present-day Cascadia subduction, which may have started out as intraoceanic subduction,(4) a lower mantle slab under Arizona and New Mexico, the last material to subduct before strike-slip motion developed along the San Andreas boundary, and (5) two narrow plate tears thousands of kilometers long, one of which is the subducted conjugate of the Mendocino Fracture Zone.

1. Motivation and Overview

[2] Seismic tomography shows that the transition zone and lower mantle under North America are dominated by anomalies that are seismically faster than average: the mantle is filled with subducted slab fragments. This is hardly surprising, given that a single large plate, the Farallon, has subducted
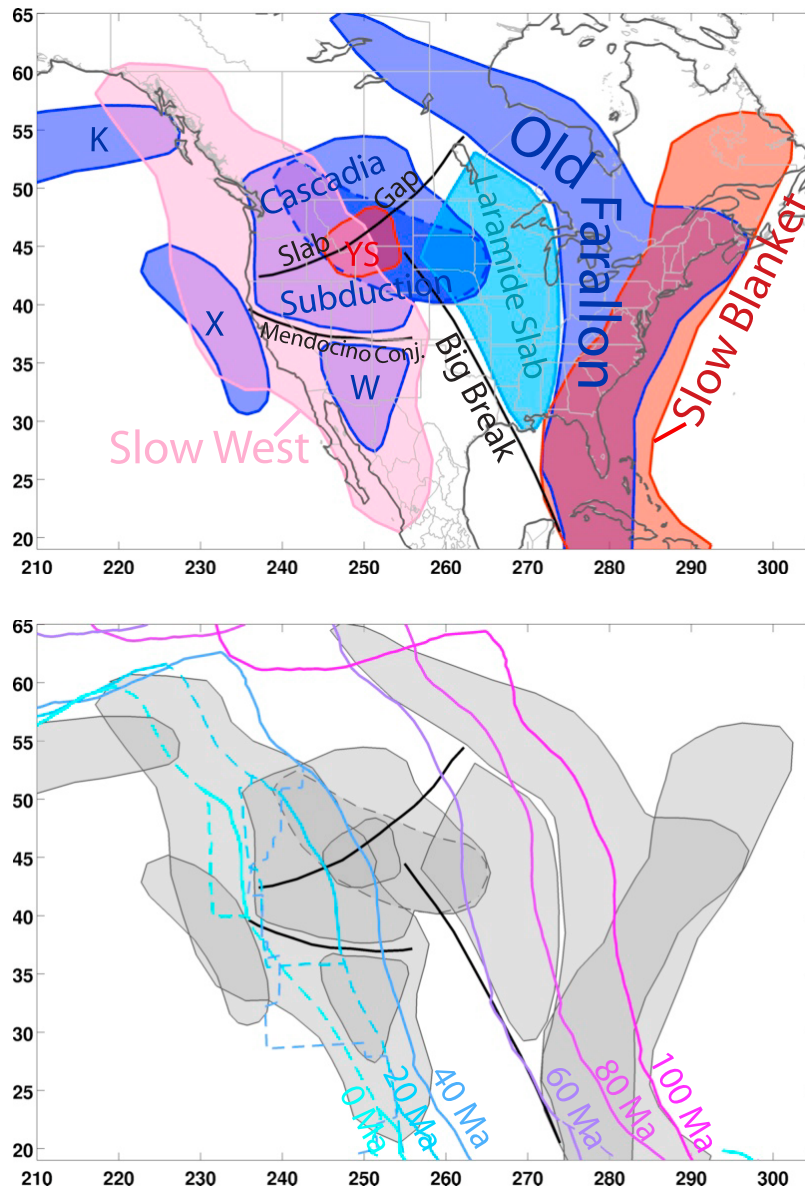
Figure 1. Mantle provinces under North America. (top) Schematic summary of large-scale structure present in the tomographic *P* wave model. The North American mantle is dominated by seismically fast anomalies (subducted slabs) at all depth levels from 0 to 1800 km down (light blue, mostly above 700 km; dark blue, mostly below). Slow anomalies do not reach much deeper than 1000 km (light red, mostly above 400 km; dark red, below 400 km). Province outlines were obtained as outlines of the anomalies seen in the "3-D maps" of Figures 9 and 10. Dashed outline inside the Cascadia province marks the deep "root" of this subduction system. (bottom) Plate motions over the past 100 Myr in an absolute frame of reference, according to *O'Neill et al.* [2005]. Line colors mark time in 20 Myr increments; solid lines are trenches and dashed lines are ridges and transform faults. Black lines are structural breaks as inscribed at top. The overarching pattern is a continuous westward migration of the Farallon-North America trench as the Atlantic Ocean kept spreading. Mantle provinces are shaded gray. If subducted material sank only vertically and tomography and tectonic reconstructions were complete and accurate, then every trench line should be overlying a fast mantle province at all times.

beneath the continent's western margin for about 200 Myr. Continuous absolute westward motion has moved the present-day North American lithosphere to overlie that former Farallon seafloor.

[3] The imaged geometry of this subducted material is complex. Structural complications, and not just on small scales, have become ever more apparent as tomographic resolving power has
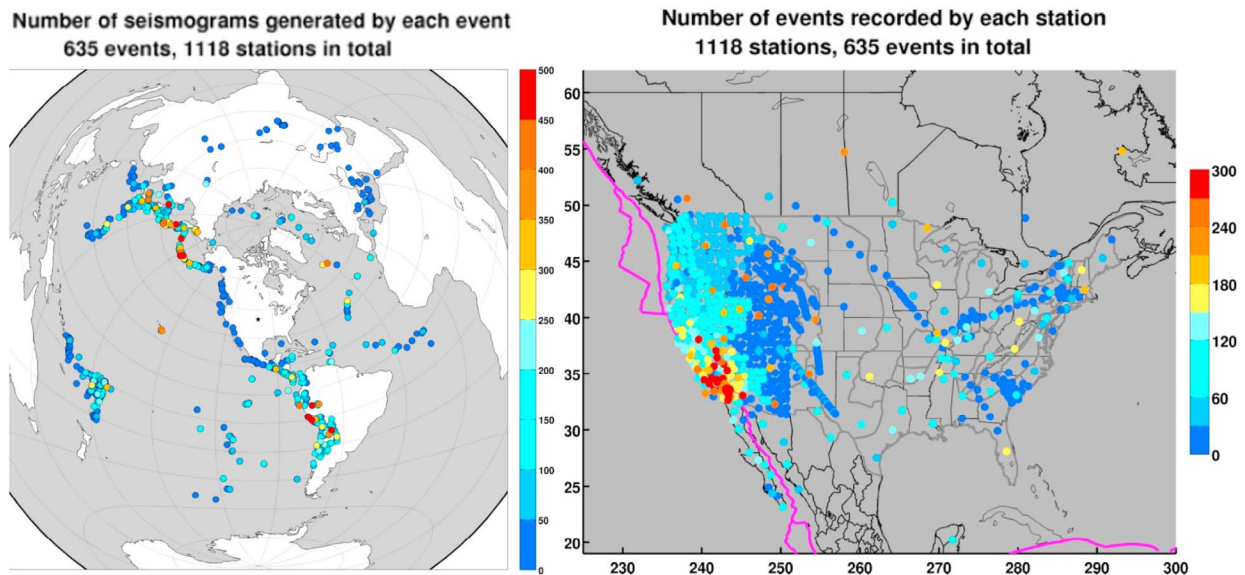
Figure 2. Source and receiver geometries of this tomographic *P* wave study. (left) Locations of the 635 earthquake sources. This is the subset of events from our global collection that generated at least 10 acceptable broadband recordings in North America at teleseismic distance range (32° to 85°). Color designates the number of stations each event was recorded at, i.e., the number of source-receiver paths per event. (This is not the number of finite-frequency measurements, which is up to 10 times larger). The azimuthal event distribution is relatively even, a favorable situation for a tomographic study. The map projection is azimuthal-equidistant; distances and directions to all places are true from the center point of projection. (right) The 1118 broadband receivers used. Color marks the number of earthquakes each station recorded at adequate quality. The dense USArray experiment in the western United States recorded relatively few events due to its time-limited deployment. It is backed by a less dense reference grid of permanent stations (red/orange), which recorded hundreds of earthquakes. Only data recorded in North America were included, and this regional data set was inverted on the global grid of Figure 4.

improved. Regional tomographies that predated the USArray seismic broadband experiment showed the currently subducting Farallon remnant (Juan de Fuca plate) in the uppermost 100–400 km near the trench. Several of these studies already observed fragmentation into smaller parts [*Rasmussen and Humphreys*, 1988; *Harris et al.*, 1991; *Bostock and VanDecar*, 1995; *van der Lee and Nolet*, 1997]. Global tomographies had picked up the deep end of the Farallon plate in the lower mantle beneath East Coast and Atlantic since at least *Grand* [1994] and *van der Hilst et al.* [1997].

[4] Those findings were still consistent with the most straightforward interpolation across the continent, a monotonously sinking, eastward dipping slab, from the west coast trench to the lower mantle beneath the Atlantic. However, this scenario is now being ruled out conclusively by newly imaged structure under the midcontinent, former gaps that the USArray has been filling rapidly since 2005 [*Sigloch et al.*, 2008; *Burdick et al.*, 2008; *Roth et al.*, 2008; *Tian et al.*, 2009; *Burdick et al.*, 2009; *Tian et al.*, 2011; *Xue and Allen*, 2010; *Schmandt and Humphreys*, 2010; *Obrebski et al.*, 2010]. Newly

imaged slab material in the transition zone and lower mantle is voluminous but fragmented, and distributed counterintuitively across depths.

[5] USArray is continuing to add detail but even now, seismic anomalies on the scale of a few hundred kilometers and larger, features termed "mantle provinces" here, are reliably identifiable to at least 1500 km depth everywhere beneath the United States, northern Mexico, and southern Canada. Indeed, the superb new data resolve not only division lines between fast and slow anomalies, but also slab tears and breaks, narrow linear hiatuses, thousands of kilometers long, between two seismically fast anomalies.

[6] Mantle province delineations serve to highlight differential evolution undergone by different elements of the convecting system. In contrast to its present jumbled state in the mantle, the Farallon plate originally evolved as one vast continuous piece of seafloor at the surface, according to plate reconstructions. Where and when did convection processes move different plate fragments onto diverging trajectories, and why?
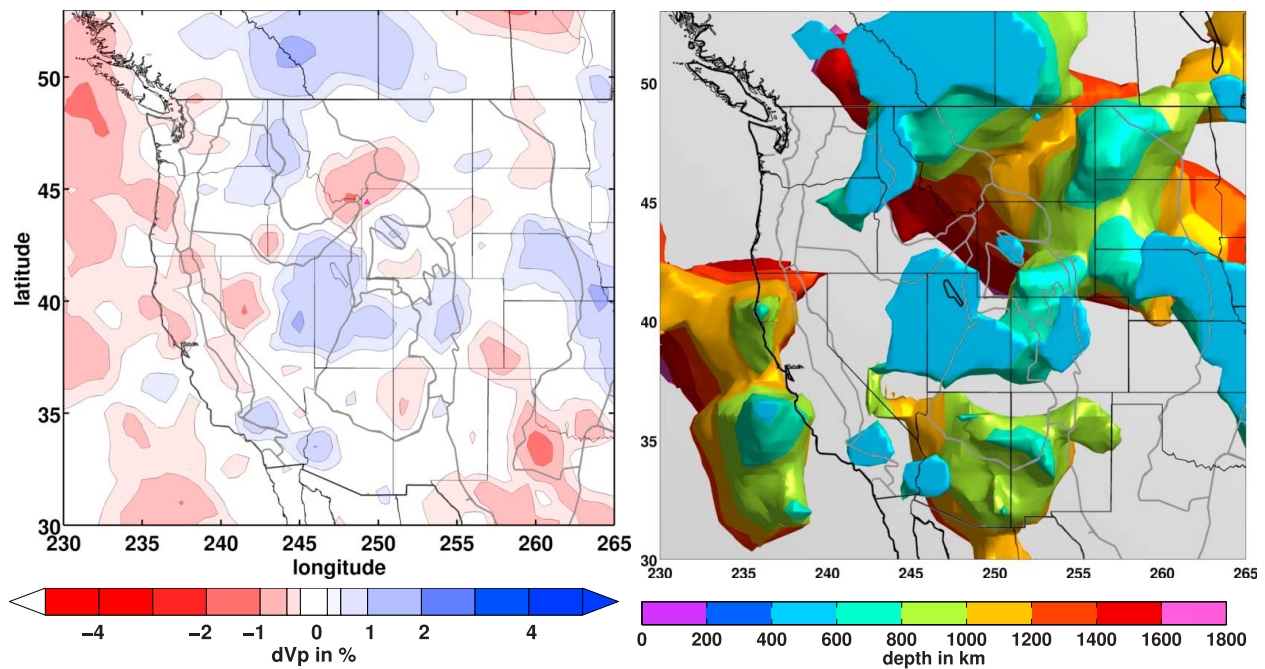
Figure 3. Side-by-side comparison of the two complementary visualization styles used to render the 3-D mantle model (all plots programmed in Matlab). (left) A conventional horizontal 2-D section, at 500 km depth under western North America. Blue indicates faster-than-average seismic velocities (with respect to the spherically symmetric background model IASPEI91) and red indicates slower. The color scale is chosen quasi logarithmic because we want to use the same color map for all depths, but the dynamic range of velocity anomalies varies strongly with depth. (right) A "color-banded 3-D map" of the same region. This map view shows structure *at and below* 500 km depth. Three-dimensional isosurfaces enclose structure that is seismically fast (by 0.35% or more); subvolumes that are slow or seismically neutral are not rendered. In order to convey proper depth perception, the scene is fully illuminated and color changes every 200 km (see color bar). The shallowest structures at 500 km depth appear as light blue patches in the foreground; their outlines correspond to the dark blue patches in the left panel. Behind them lies structure at 600–800 km depth (turquoise), 800–1000 km depth (light green), 1000–1200 km (yellow), and so on. Any slow structure, which is red in the left panel, is missing completely. Fast structures at these midmantle depths imply subducted slabs. This particular 3-D map opens a view onto the subterranean landscape created by the subducted Farallon plate. It is a tomographer's equivalent of preparing a fossil out of its rock matrix.

[7] The core of this paper offers a descriptive survey of seismic mantle provinces imaged under continental North America, with an emphasis on the transition zone and deeper. Figure 1 shows a schematic overview of those provinces. I attempt a reconciliation of the imaged assemblages with tectonic plate reconstructions and with first-order surface observations. This synopsis yields many consistencies across the independent observations, which increase confidence in the modeling abilities of the different disciplines involved. It also hits some serious contradictions that spotlight shortcomings in current understanding, but will hopefully provide leverage points for their remediation.

[8] The tomographic *P* wave model presented here is an extended version of the one given by *Sigloch et al.* [2008]. Besides all of the contiguous United States, it now covers large parts of Mexico and most of Canada (though upper mantle resolution

is poor under northern Canada, due to lack of recording stations). The mantle model may be downloaded as auxiliary material.[1]

[9] Section 2 describes the inversion method and the new kind of data used, systematically frequency-dependent measurements of traveltimes and amplitudes, combined with finite-frequency modeling. As the full extent of three-dimensional complexity in the mantle models became apparent, I experimented extensively with 3-D visualization and converged on a new technique I call "color-banded 3-D maps," which is explained in section 3. Section 4 discusses image resolution using the 3-D maps. Sections 5 and 6 survey the mantle provinces under Eastern and Western North America, respectively. For readers interested only in the imaging results and their tec-
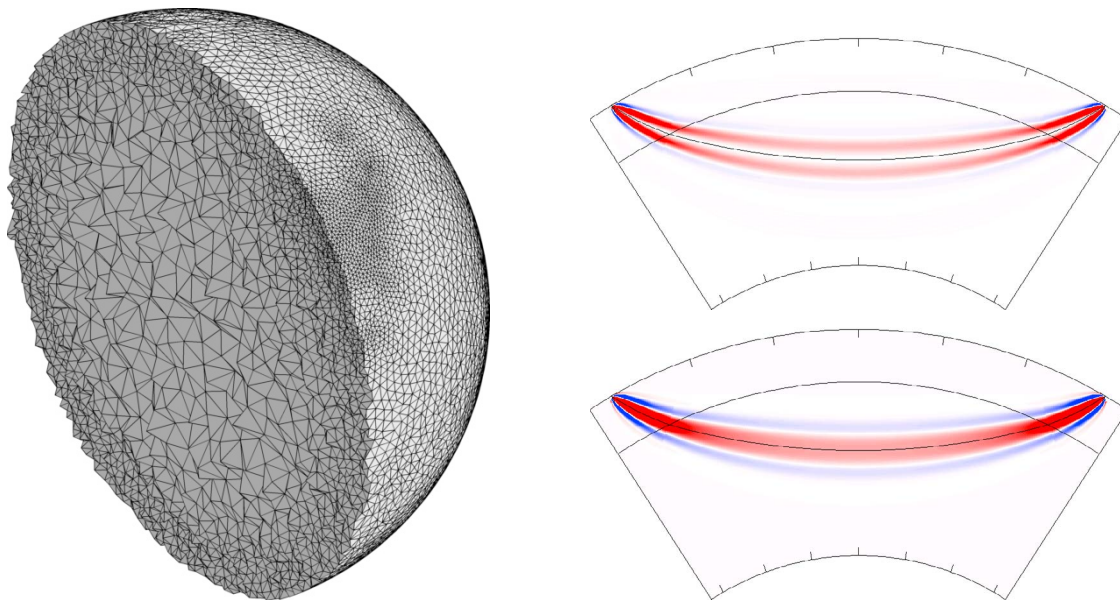
Figure 4. (left) Half of the global tetrahedral mesh used for inversion. Irregular tetrahedra adapt to the expected model resolution, as a function of depth and location. The finely meshed area is eastern North America. In the upper mantle, tetrahedra facet length varies between 65 km and 200 km. Below, it gradually increases to 500 km at the center of the earth. The volume of a typical tetrahedron is 5 to 7 times smaller than the volume of a cube of equal facet length. (right) Vertical mantle sections showing typical Fréchet sensitivity kernels [*Dahlen et al.*, 2000; *Dahlen and Baig*, 2002], which get mapped onto the mesh by numerical quadrature. Shown is a *P* wave traveltime kernel ("banana-doughnut kernel" with the characteristic central hole) and an amplitude kernel, both with a dominant period of 15 s and an epicentral distance of 60°. Red and blue are positive and negative sensitivities, respectively. The central black ray is the hypothetical sensitivity of an infinite-bandwidth measurement, which is the ray theoretical approximation.

tonic interpretation, sections 5 and 6 together with the captions of Figures 1–12 allow for a fairly self-contained reading.

2. Data and Tomography Method

2.1. Finite-Frequency Modeling Using True Finite-Frequency Data

[10] The imaging method used, multifrequency tomography, could be characterized as "second generation" finite-frequency technique. The advanced computational modeling of *Dahlen et al.* [2000] and *Hung et al.* [2000] is combined with exactly the kind of frequency-dependent data that it was envisioned for *Sigloch and Nolet* [2006]. Finite-frequency tomography is a waveform-based inversion method that is computationally affordable across the whole frequency spectrum that nature presents us with. Currently this is not the case for any other waveform tomography method, at least not for body waves on a global scale.

[11] Unlike classical ray theory, finite-frequency modeling embraces the wave nature of broadband seismograms and does not attempt to conceptually reduce them to sequences of propagating delta pulses. Wavelength-dependent phenomena are explicitly modeled, and the data are processed accordingly [*Sigloch and Nolet*, 2006]. Early global finite-frequency tomography [*Montelli et al.*, 2004b, 2004a] could not exploit the full power of the method, for lack of properly generated, frequency-dependent data sets. Finite-frequency observables are not limited to time delays [*Dahlen and Baig*, 2002; *Dahlen*, 2005], for example, the present study and *Sigloch et al.* [2008] also invert amplitude anomalies as a technical novelty.

[12] In contrast to numerical forward methods for full waveform propagation [e.g., *Komatitsch and Tromp*, 1999; *Nissen-Meyer et al.*, 2007; *Jahnke et al.*, 2008; *Fichtner et al.*, 2009; *Käser and Dumbser*, 2006; *Akcelik et al.*, 2007; *Virieux and Operto*, 2009], the computational cost of finite-frequency modeling as conceived by *Dahlen et al.* [2000] does *not* grow with frequency. Wave scattering is modeled extremely efficiently by exploiting the almost spherical symmetry of the real earth, and by synthesizing the total scattering field from
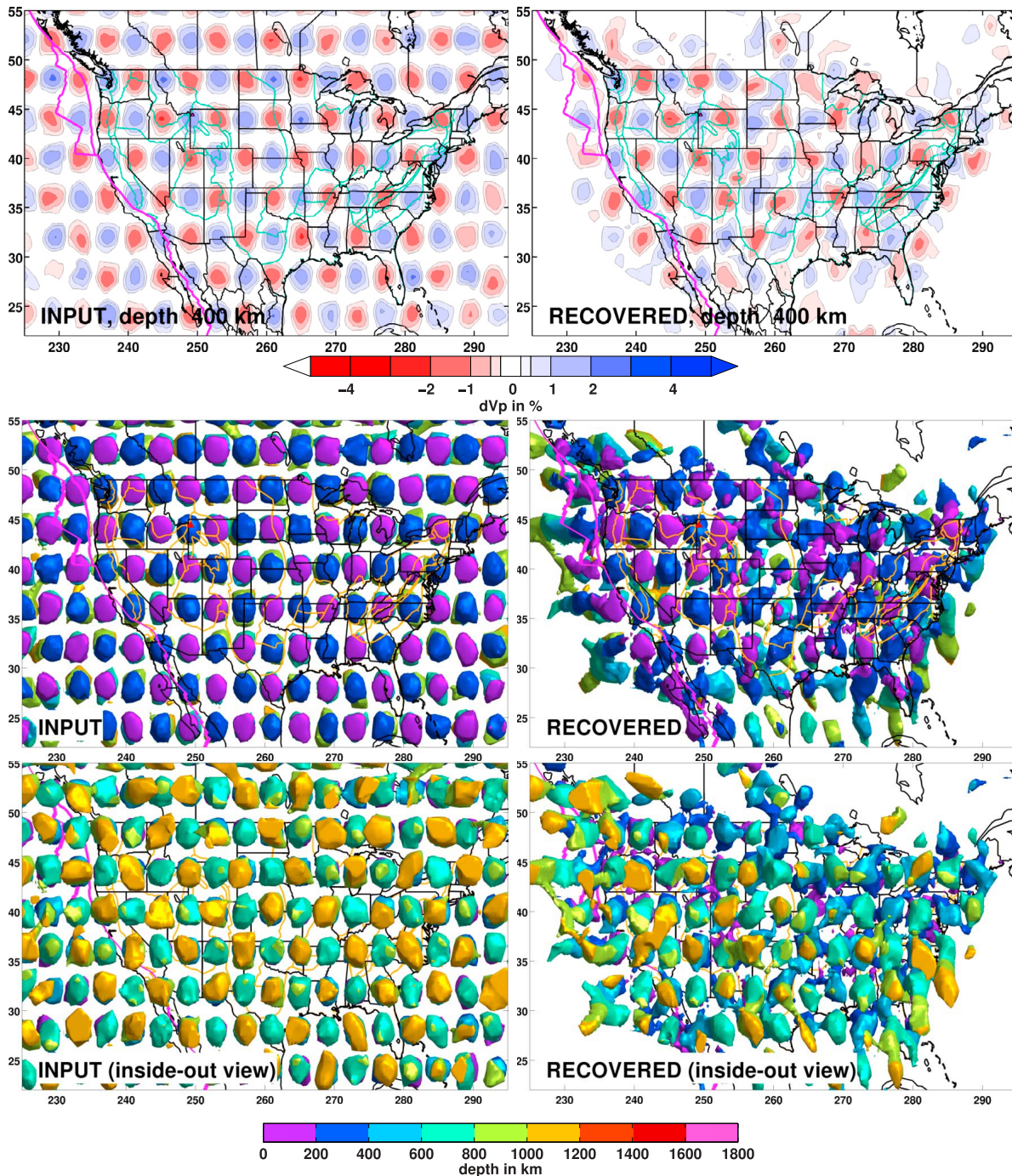
Figure 5. Resolution test. The input pattern is a grid of spheres (three-dimensional Gaussian pdfs) of 200 km diameter and peak value $dV_p/V_p = \pm3\%$. Left column shows input patterns, and right column shows output patterns retrieved by the inversion (using realistic regularization and noise). (top row) A 2-D section at 400 km depth. The irregular grid nicely renders the spheres of 200 km diameter (top left). The spheres are retrieved very well in the densely instrumented western United States, but less well in the central United States, and not at all under the ocean basins and parts of Canada (top right). (middle and bottom rows) Color-banded 3-D maps showing the same resolution test. Only the slow spheres are rendered, at isosurface threshold $dV_p/V_p = -0.35\%$. The middle row shows an ordinary map view. Spheres positioned at 200–400 km depth (purple, blue) are visible in the foreground; beneath the central United States, they are imperfectly resolved. The bottom row shows an "inside-out view," which reverses background and foreground so that the deepest structures emerge toward the viewer (similar to an observer sitting at the center of the earth, looking up). The deepest layer of 200 km spheres was positioned around 1100 km depth (yellow). They are still resolvable under some parts of the continental United States.
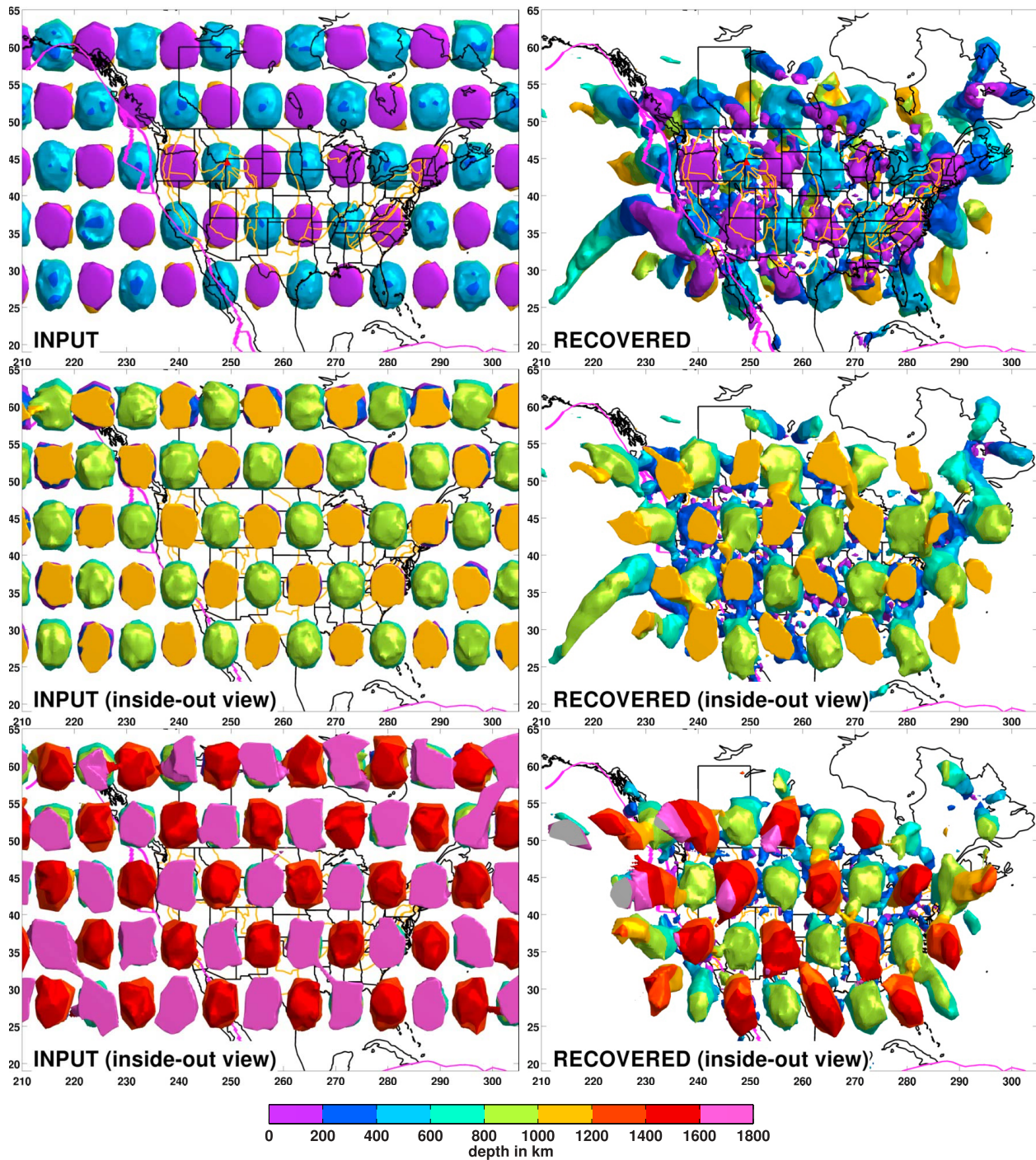
Figure 6. Resolution test. Like Figure 5, except that test spheres of twice the diameter (i.e., 400 km) are used. (top row) A 3-D map view. (middle and bottom rows) "Inside-out views." In the middle row, the test function input extended to 1100 km depth and is decently retrieved under all of the continent. In the bottom row, test functions extended to 1800 km depth (pink) and cannot be retrieved properly at the largest depths. (In reality, the situation is more favorable than the rendering may suggest. Structure is actually retrieved, but at a much weaker magnitude than the input. This is not apparent from the rendering because isosurface thresholds are chosen identical for input and output, at $dV_p/V_p = -0.35\%$.) Inside-out views are helpful for assessing the depth resolution limit, and the extent of artificial smearing to deeper depths. The diagonal streaking artifacts out into the ocean basins are also present in the actual mantle model.
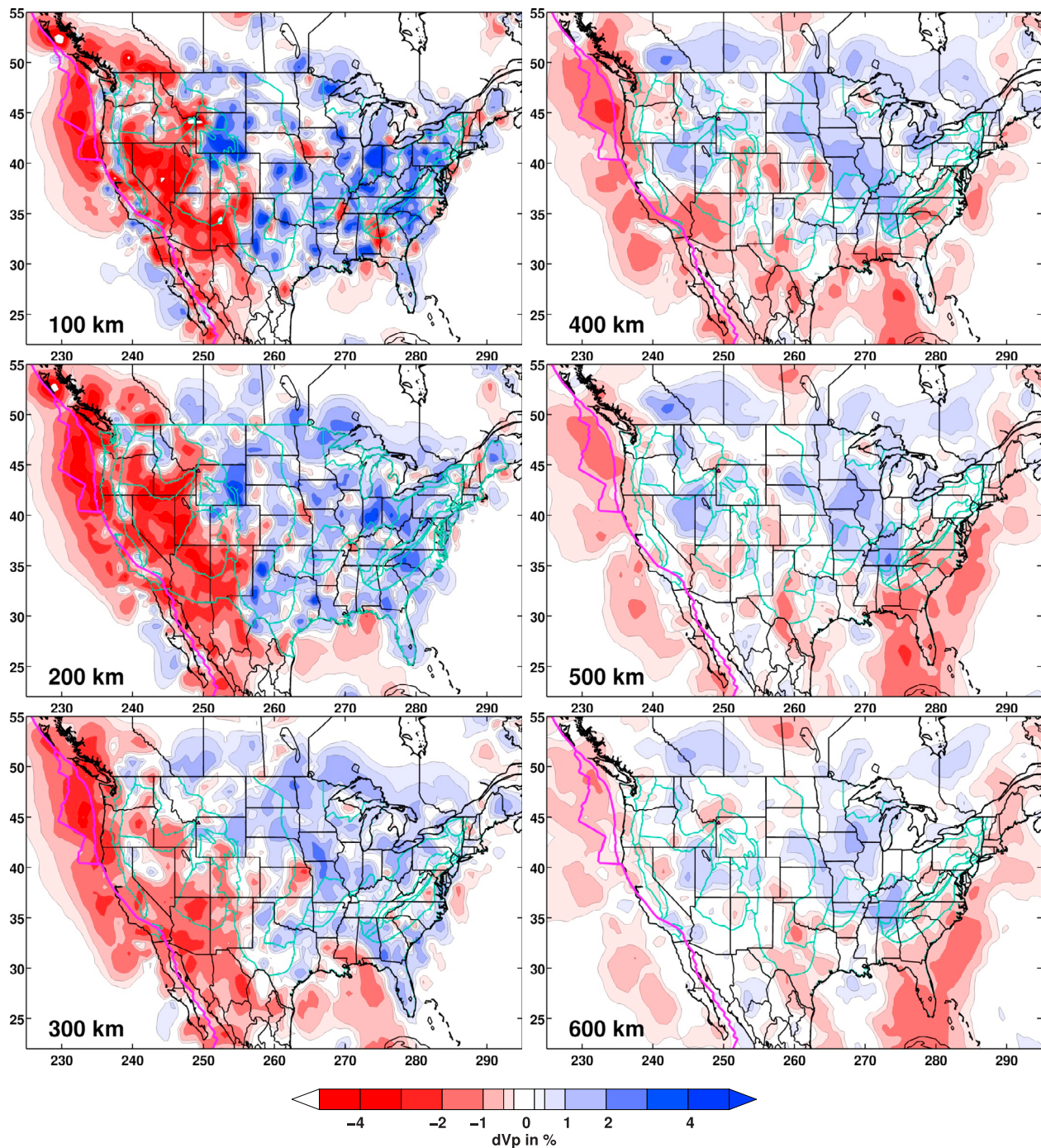
Figure 7. *P* wave velocity anomalies dV_p/V_p in the upper mantle under North America. Horizontal sections are shown at depth increments of 100 km. The radially symmetrically reference model is IASPEI91. Velocity anomalies in the upper mantle are on the order of several percent.

point scatterers in the Born approximation, using paraxial ray tracing. This computational efficiency makes for the method's competitive edge in modeling the highly resolving, short-wavelength body waves (but in practice also surface waves) [e.g., *Zhou et al.*, 2004]. Its inherent limitations compared to more complete forward methods (e.g., failure to account for

wave diffraction) are of no concern when direct teleseismic body waves are investigated, such as here.

2.2. Data Processing

[13] Rigorous quality control of the raw broadband waveforms and deconvolution of the source time
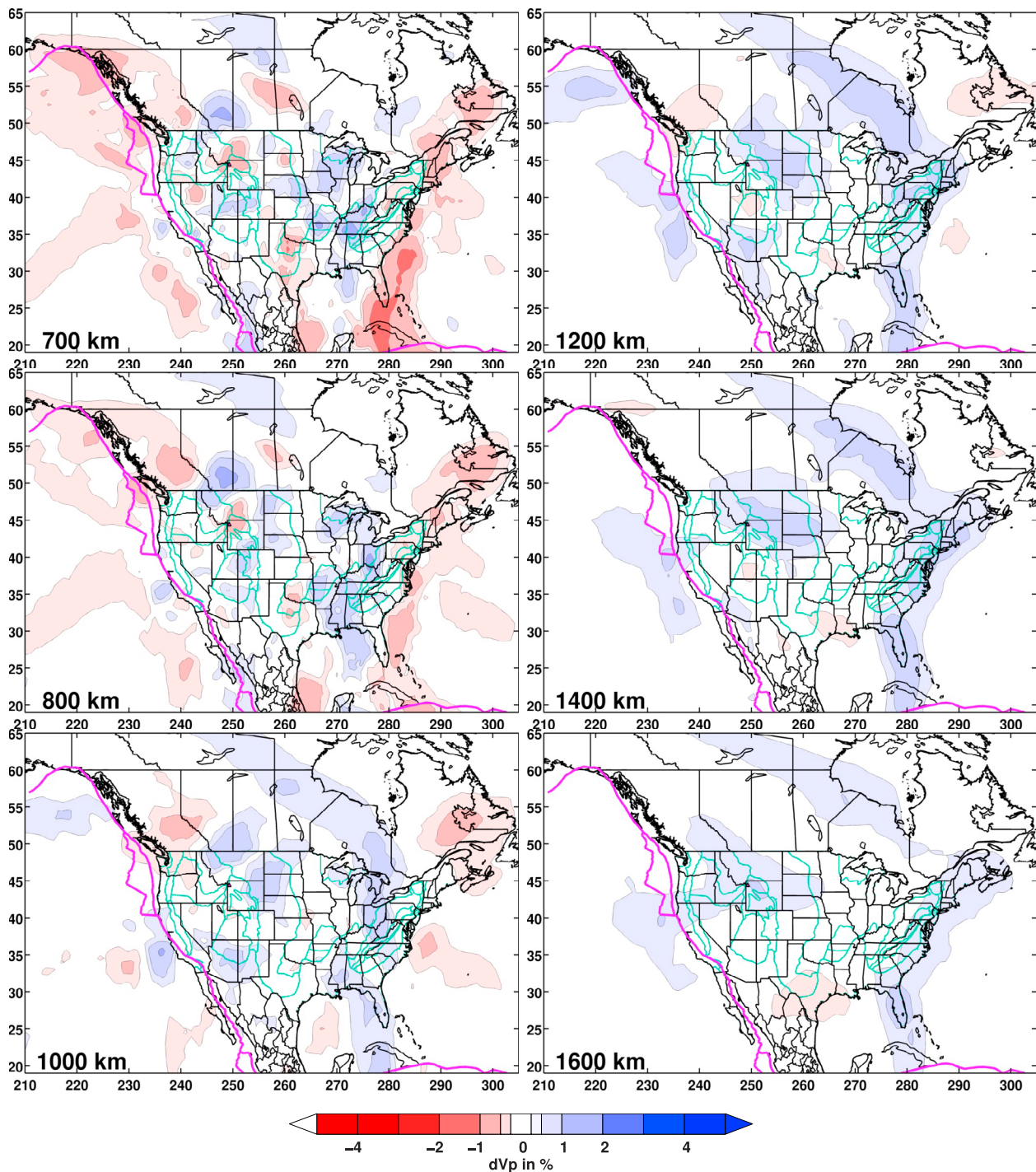
Figure 8. P wave velocity anomalies dV_p/V_p in the lower mantle under North America. Sections are shown at 700 km, 800 km, 1000 km, 1200 km, 1400 km, and 1600 km depth. Note that the map limits are somewhat wider than in Figure 7. Lower mantle velocity anomalies are on the order of one percent.

function are preprocessing steps in the generation of multifrequency traveltimes and amplitudes [*Sigloch and Nolet*, 2006]. I did a comprehensive survey of global seismicity between 01/1999 and 08/2007 and included all usable broadband waveforms measured in North America, in total 59,800 source-receiver

paths generated by 635 earthquakes and recorded at 1118 stations. Figure 2 shows the earthquake and station coverage.

[14] Each source-receiver path produces up to seven finite-frequency traveltime anomalies, and
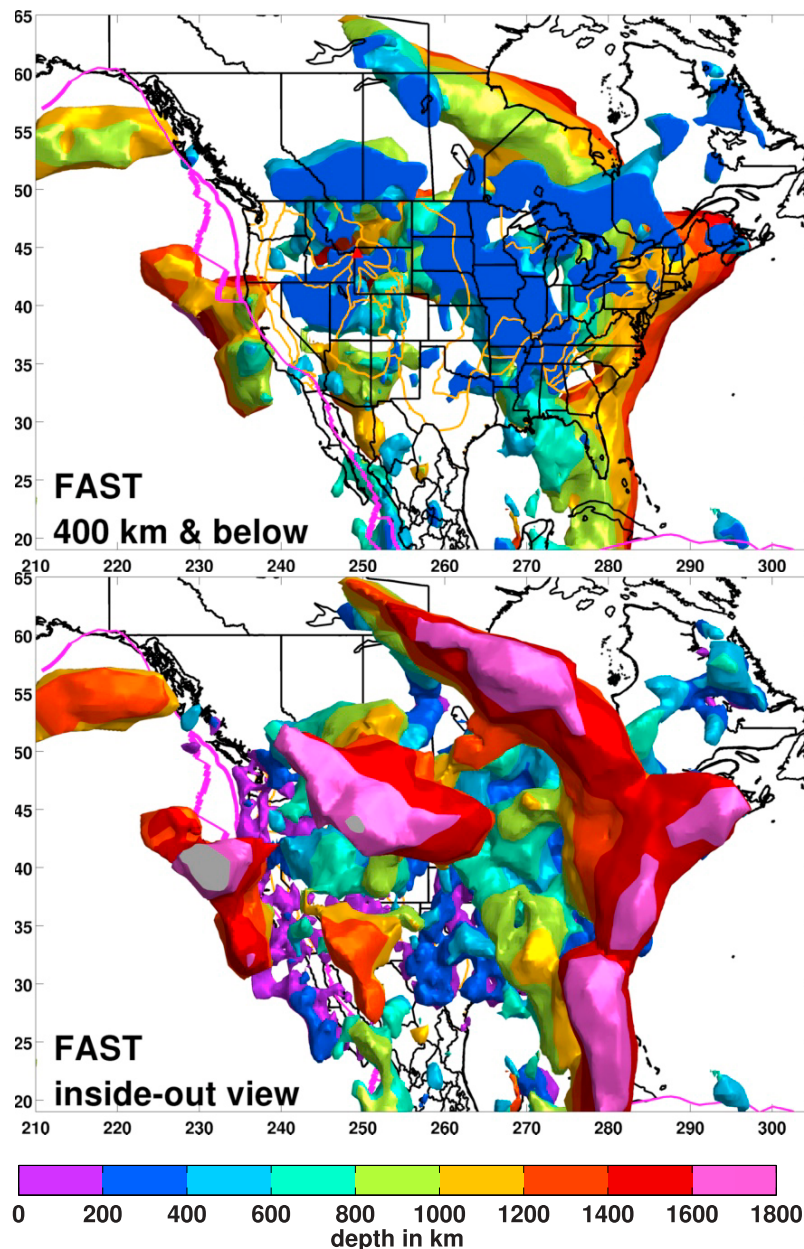
Figure 9. Seismically *fast* structure under North America, shown as color-banded 3-D maps. The isosurface threshold is $dV_P/V_p = +0.35\%$. (top) A map view of all fast anomalies *at and below* 400 km depth (the uppermost mantle is excluded because the fast lithospheric lid under most of North America would obscure the view on deeper structure). The structure at exactly 400 km depth is dark blue, while the structure immediately below is light blue. The red triangle marks the location of the Yellowstone hot spot. (bottom) An "inside-out" view of fast structure at *all* depth levels; the deepest structure emerges to the foreground, and the purple lithosphere is moved to the background. Note the following imaging limitations and artifacts: for the deepest structures (pink), simultaneous smearing into depth and loss of resolution (they may or may not extend even deeper); no resolution in the middle of the ocean basins; gradual loss of resolution north of 55°N. Refer to the resolution tests for details.

up to three finite-frequency amplitude anomalies: observed and modeled broadband waveforms are filtered through a bank of passband filters before measuring time delays and amplitudes by cross correlation [*Sigloch and Nolet*, 2006; *Sigloch*, 2008]. This procedure exactly reflects the definition of finite-frequency sensitivity kernels by *Dahlen et al.* [2000]. For the filtering I use Gabor filters, which are Gaussians in the log-frequency domain; their constant fractional bandwidth is chosen to be
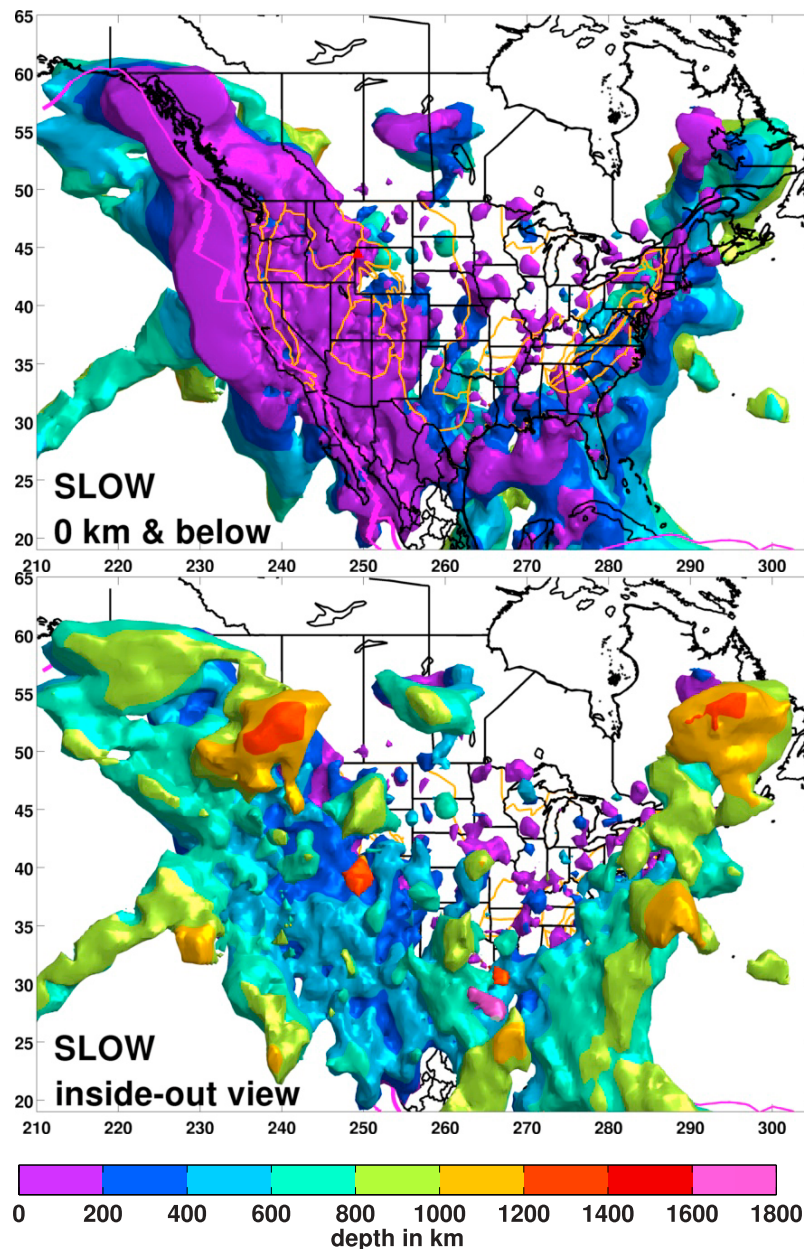
Figure 10. Seismically *slow* structure under North America, shown as color-banded 3-D maps. The isosurface threshold is $dV_P/V_p = -0.35\%$. (top) A map view of slow anomalies *at all depth levels*. (bottom) An "inside-out" view of the same structure. In general, slow anomalies do not extend much deeper than 1000 km, unlike fast anomalies. Note the following imaging limitations and artifacts: between 30°N and 40°N, a SW-NE streaking wave path artifact across the Pacific and a weaker NW-SE striking one across the Atlantic; the deep (red) anomaly around 53°N, 240°W may not extend quite as deep in reality (downward smearing in resolution tests); questionable deep anomaly around 53°N, 290°W (see text); gradual loss of resolution north of 55°N; no resolution in the mid-ocean basins. Refer to the resolution tests for details.

one octave (a factor of two). The seven passbands have dominant periods of 21.2 s, 15.0 s, 10.6 s, 7.5 s, 5.3 s, 3.8 s, and 2.7 s. For amplitudes, only the three lower bands were used. Hence the information content of each broadband seismogram gets condensed into ten robust scalars (as opposed to just one scalar in ray theoretical modeling). In total, 369,827 finite-frequency traveltime measurements and 160,027 amplitude data were deemed acceptable (cross-correlation coefficients between data and synthetic seismograms in excess of 0.85 and 0.9, respectively).
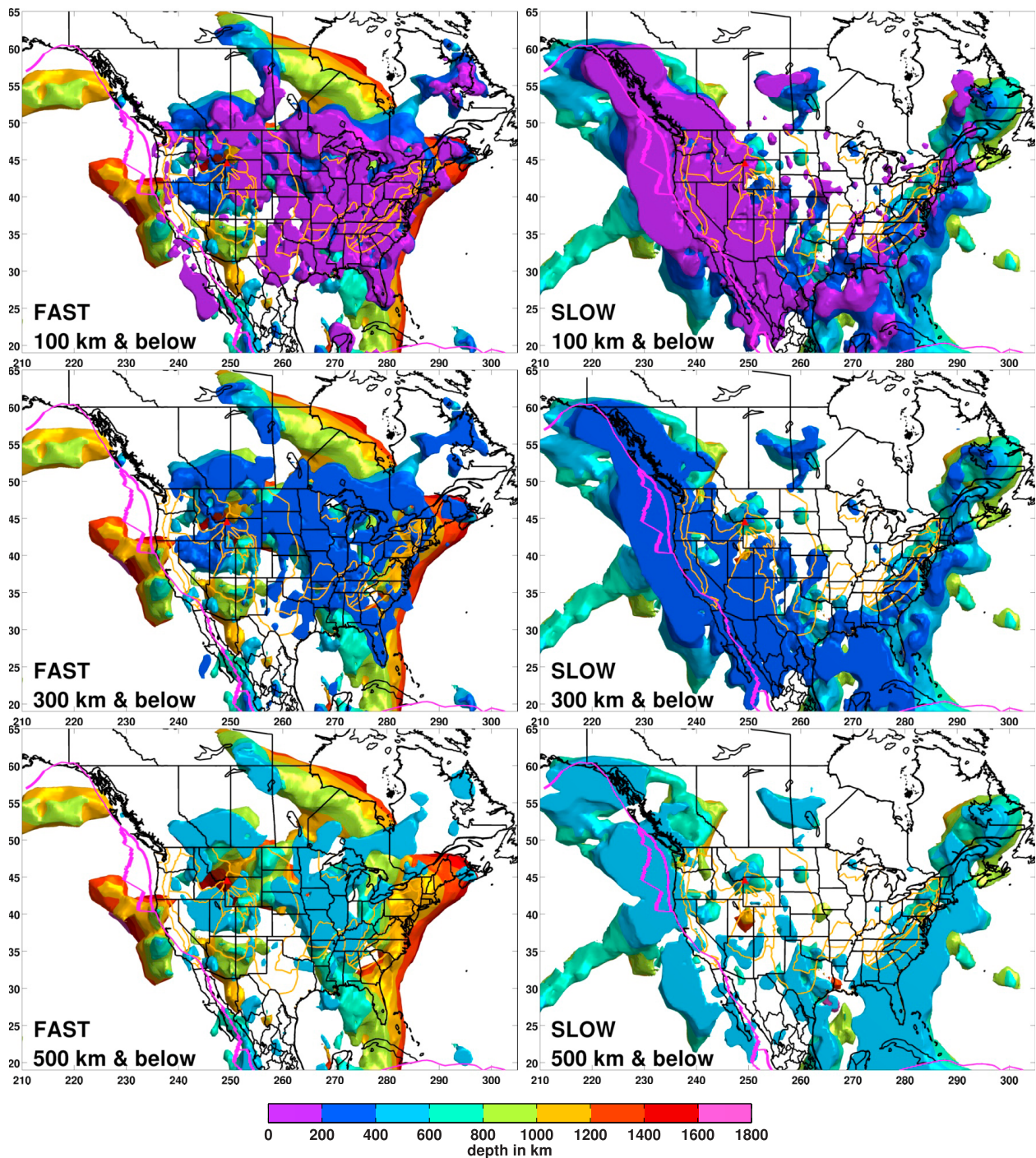
Figure 11. Side-by-side comparison of fast structure (first column, isosurface threshold dV_p/V_p = +0.35%) and slow structure (second column, dV_p/V_p = −0.35%). (top row) 3-D map showing structure at and below 100 km depth. (middle row) At and below 300 km depth. (bottom row) At and below 500 km depth.

[15] At the high-frequency end, the challenge is to achieve a good cross-correlation fit while detecting and excluding spurious cycle skips. At the lowest frequencies, the accuracy of the cross-correlation deteriorates (earthquakes used are rarely larger than magnitude 7.0 and can be as small as 5.6), and the corresponding sensitivity kernels do not add much in terms of resolution. Each passband datum gets modeled by a traveltime kernel [*Dahlen et al.*, 2000] or an amplitude kernel [*Dahlen and Baig*, 2002], using the software of *Tian et al.* [2007] for the computations. The kernels are computed
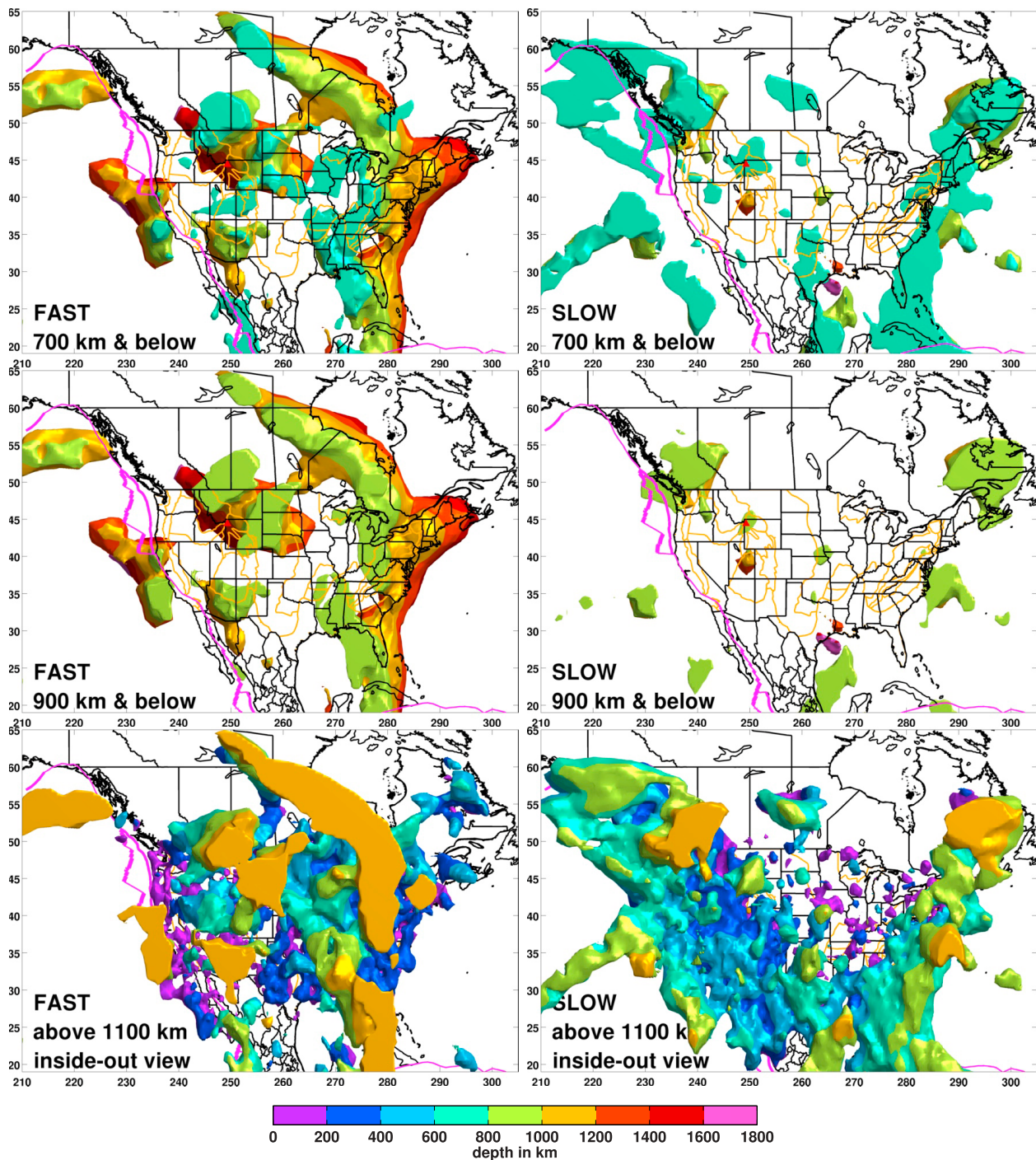
Figure 12. Continuation of Figure 11. (top row) Structure at and below 700 km depth. (middle row) At and below 900 km depth. (bottom row) An inside-out view, showing only structure *above* 1100 km depth.

through the spherically symmetric reference model IASPEl91 of *Kennett and Engdahl* [1991].

2.3. Inversion

[16] All frequency-dependent observables are required to *jointly* fit the *P* velocity model. The wavelength-

dependent scattering effects captured by the finite-frequency processing amount to more constraints on mantle structure: any given source-receiver path is constrained by up to ten observations, whose sensitivity kernels of varying width and internal shape discriminate between potential locations of heterogeneity. Amplitude data can in principle also con-

strain seismic attenuation. In practice, we could not obtain a stable attenuation model from the teleseismic *P* waves, since the dominant cause of *P* wave amplitude anomalies turns out to be focusing, i.e., elastic structure [*Sigloch*, 2008; *Sigloch and Nolet*, 2008].

[17] For regularization, we use a chi-squared criterion with a mix of second-derivative smoothing and norm damping. The preferred model's normalized χ^2 misfit is 20% higher than that of the unregularized solution. The data residuals after inversion have standard deviations of 0.43 s for traveltime anomalies dT (jointly in all frequency bands) and 0.18 for amplitude anomalies $dA/A - 1$.

[18] I directly compared finite-frequency inversion (of all multifrequency data) with ray theoretical inversion (of only broadband data), using the same regularization strategy and solving to the same misfit. In agreement with theoretical expectations and with similar investigations by *Montelli et al.* [2004a] and *Hung et al.* [2004], I observe that finite-frequency tomography is less sensitive to the exact type of regularization (the solution is less ambiguous), and resolves more structure at deepest depths and toward the uninstrumented ocean basins (thanks to the spatially widened measurement sensitivities and their correct treatment of wave scattering).

[19] In the finite-frequency model, the retrieved mantle anomalies are up to two times larger in magnitude, especially in the lower mantle [*Sigloch*, 2008, chapter 2]. They are also stronger than in ray theoretical models by other authors who used largely the same data [e.g., *Burdick et al.*, 2009; *Roth et al.*, 2008]. My direct method comparison suggests that the stronger mantle heterogeneity is real, rather than some arbitrary effect of regularization. Ray theory is expected to underpredict mantle heterogeneity because it neglects wavefront healing: a weak traveltime anomaly is invariably interpreted to be caused by weak mantle heterogeneity. By contrast, methods that account for wave scattering may diagnose either a weak and shallow structure, or a strong but deep structure. For quantitative interpretation in terms of mantle dynamics, it is important to correctly capture not just the patterns of mantle heterogeneity but their absolute magnitudes as well.

[20] Correcting for uncertain crustal structure poses the same issues as in traditional ray theoretical inversions, since this multifrequency tomography operates within a spectral range in which crustal finite-frequency effects are not thought to be strong [*Zhou et al.*, 2003; *Ritsema et al.*, 2009]. I apply a priori crustal corrections predicted by model CRUST2.0 [*Bassin et al.*, 2000]. Its uncertainties and limited spatial resolution imply that the uppermost 100–150 km of a teleseismic inversion should be taken with a grain of salt. Given my focus on the transition zone and below, this caveat becomes relevant only in a few instances, e.g., the discussion of the asthenosphere under the western United States. There however, traveltime anomalies are too strong and spatially variable to be attributed mainly to misestimation of the crust. The alternative treatment, allowing for free stations corrections, would not be preferable, as it can inadvertently absorb an almost arbitrary amount of signal from the mantle. I do allow for free parameters to mitigate the effects of mislocated earthquake sources ("event corrections"), with a priori parameter uncertainties of 8 km per spatial direction, and 2.0 s for the origin time. More technical detail regarding the inversion can be found by *Sigloch* [2008, chapters 2 and 4], *Tian et al.* [2009], and *Tian et al.* [2011].

3. Visualizing 3-D Velocity Structure

[21] Conveying the information content of volumetric tomography models in flat, still pictures is a challenge. Figure 3 introduces the two complementary visualization techniques used here. Two-dimensional sections at a fixed depth, in shades of red (seismically slow) and blue (seismically fast), are the tried-and-tested style. For the sake of visual contrast, the color scale is chosen quasi logarithmic, with more rapid color changes around the average. The lateral average itself ($dV_p/V_p = 0$) at any depth is the *P* velocity specified by reference model IASPEI91 of *Kennett and Engdahl* [1991]. Velocity anomalies are so much stronger in the upper than in the lower mantle that a linear color scale would result in color saturation everywhere at shallow depths, or in very dim contrast deeper down.

[22] When geometries are very three-dimensional, assembling a mental picture of the volumetric connectivities is difficult, even when many 2-D sections are shown. "Color-banded 3-D maps" are a plotting style I developed to address this problem. They are three-dimensional contour renderings of velocity isosurfaces, 3-D surfaces rendered at a constant anomaly threshold. I choose $dV_p/V_p = +0.35\%$ for seismically fast structure (slabs and lithosphere, e.g., Figure 3, right), and $dV_p/V_p = -0.35\%$ for slow structure.

[23] Reasonable choices of this threshold are between 0.25% and 0.5%, and within that range the structural appearance changes only modestly. These rather low absolute values are set by mid-mantle structure, which simply does not feature anomalies much in excess of $dVp/Vp = 1\%$ (see *Schuberth et al.* [2009] for a review). Note that a weak contour threshold does not distort upper mantle structure, where velocity gradients are large and fast-slow transitions so localized that any threshold in the rough vicinity of zero produces much the same isosurfaces.

[24] Most 3-D maps render either only fast or only slow structure. This avoids visual overload, and color need not be expended on signaling the sign of velocity anomalies. Instead it is freed up to code for their depth, an important visual aid because the brain must somehow disambiguate between depth and lateral distance in the projected scenes.

[25] The 3-D scene is fully illuminated to convey perspective. It could be displayed from any oblique angle, but here I prefer map views (viewing direction vertically downward), for direct comparison to the traditional 2-D map sections, as demonstrated by Figure 3. Most color-banded 3-D maps render only structure *below* a certain depth. This opens a window on deeper structure by masking out the very heterogeneous upper mantle.

[26] The overall effect of 3-D contour plots is to deemphasize internal velocity gradations of mantle provinces ("somewhat fast" versus "very fast"), and to emphasize their structural continuity, also and especially across depths. Structural breaks, such as a narrow, oblique slab tear from the upper to the lower mantle, spring out from the isosurface renderings, a clear advantage for the structural-geology-like discussion attempted here.

4. Spatial Image Resolution

[27] Figure 4 (left) shows the discretization of the globe used to solve the inverse problem numerically. As a continuously variable mesh of irregular tetrahedra, it locally adapts to the data density and thus to the expected local image resolution. The mesh is generated by the free DISTMESH software of *Persson and Strang* [2004]. Of the 92,175 global grid nodes, approximately 18,000 are located under North America. The quasi-analytical sensitivity kernels are cast onto this mesh by numerical quadrature. The interpolation functions are centered on the nodes and taper off linearly toward the nearest neighboring nodes.

[28] Figures 5 and 6 show resolution tests, plotted as conventional red-blue sections and as color-banded 3-D maps. The test patterns are regular grids of spheres, i.e., three-dimensional Gaussian density functions with a standard deviation ("diameter") of 200 km and 400 km. The resolution test inputs can also be regarded as rendering tests, which show the capacity of the irregular mesh to render regular spheres. Features too fine for the grid to render are obviously not resolvable by the inversion either. Test functions of 200 km diameter are rendered cleanly everywhere in the upper mantle but not in all of the lower mantle (Figure 5, middle left versus bottom left). 400 km spheres are decently rendered everywhere under North America.

[29] In practice, fine 3-D meshes easily run up against hardware limitations because the sensitivity matrix must be held in memory during the (parallelized) inversion, and finite-frequency kernels are much less sparse than ray theoretical ones. By inverting on incrementally finer meshes, I verified that the presented mesh does not artificially limit the inherent resolution capacity of the data.

[30] The right columns of Figures 5 and 6 show structure retrieved by the inversion test. I used the same regularization settings as for the real data, and the same signal-to-noise ratio (3.5 for traveltime data, 1.2 for amplitude data, added noise is white and Gaussian).

[31] Ocean basins and near-surface structure are least resolved by body wave tomography, for lack of crossing wave paths. Under all of the United States, resolution is good from the transition zone down to 1500–1800 km depth. In the western quarter, resolution is excellent from the surface down, thanks to USArray. In the eastern quarter, the upper few hundred kilometers are also well resolved. A fair number of Mexican stations are available through IRIS-DMC (where all data came from), so resolution is quite good from the transition zone down. Canada offers very few stations, but under southern Canada transition zone and midmantle are still decently resolved, thanks to seismicity recorded in the United States and to the "fat" banana-doughnut kernels. A similar extension of range applies to the first few hundred kilometers offshore from the coasts. An obvious imaging artifact appears as diagonally streaking wave path beneath the Pacific Ocean, which is also present in the actual mantle models of Figures 9 to 12. To a lesser extent, oceanward smearing is also apparent on the Atlantic side.

[32] Note the "inside-out" viewing style for some of the 3-D maps. For example, exactly the same structure is rendered in the middle and bottom rows of Figure 5, but in the latter, foreground and background are reversed. Hence the deepest structure seems to stick out toward the viewer. This reversal of the z axis amounts to taking the viewpoint of an observer at the center of the earth, looking up toward the surface (except that north and south would also appear flipped in such an experiment).

5. Mantle Provinces Under Eastern North America

[33] All plots from Figure 7 onward display the same tomographic model in complementary ways. Figures 7 and 8 are 2-D sections at various upper and lower mantle depths. A central position is occupied by the large 3-D maps of Figures 9 (fast structure) and 10 (slow structure). Most features discussed in the text are readily seen in Figures 9 and 10, and the schematic mantle province outlines of Figure 1 were derived from them. The systematic depth sequences of 3-D maps in Figures 11 and 12 are useful for better assessing the depth extent of individual provinces.

[34] I discuss the mantle provinces featured in Figure 1, proceeding from east to west. This implies old to young, since the Farallon trench made a westward sweep across the study area over the past 100 Myr. The term "Farallon trench" subsumes convergent margin segments with North America that arose from fragmentation of the Farallon plate proper, including the Kula plate between roughly 80 and 40 Myr, and the Juan de Fuca plate since 30 Myr.

[35] Comparison of Figures 9 and 10, especially the inside-out views, shows that volumes of seismically fast material predominate. Fast anomalies reach much deeper and can be found at any depth between 0 and 1800 km (the lower limit of image resolution), whereas slow anomalies are limited to the upper 1000 km. Fast anomalies can be taken to mean lithosphere in the upper 200–300 km, but at deeper depths they imply cold subducted slab material. My first-order approach to spatial and temporal orientation is as follows. If (1) a piece of plate sinks purely vertically after entering the trench (i.e., dominant effect of gravity, lateral motion negligible), (2) the tomographic model is complete, and (3) the tectonic reconstruction is complete and accurate to within the uncertainties of the tomography, then all paleotrench lines should overlie a present-day fast mantle province. No trench line should overlie a mantle column that is neutral or slow at all depths. In cases of mismatch, I consider which assumption is most likely violated. On coarse spatial scales, vertical sinking of slabs has long been recognized as a good approximation, most evidently in the match of circum-Pacific fast seismic anomalies to paleotrench locations. Largely vertical sinking has been confirmed by many modeling studies [e.g., *Christensen*, 1996; *Steinberger*, 2000, and references therein; *Goes et al.*, 2008]. The question is at what scale, if ever, the errors in this assumption exceed the uncertainties of the seismic or tectonic models.

[36] I discuss *O'Neill et al.* [2005] as exemplary plate model, which uses a moving Atlantic-Indian Ocean hot spot reference frame. I also considered reconstructions by *Engebretson et al.* [1985] and *Müller et al.* [1993], using the GPlates software by *Boyden et al.* [2011] and M. Gurnis et al. (Global plate reconstructions with continuously closing plates, submitted to *Computers & Geosciences*, 2010); however, the (in)consistencies encountered remained quite similar.

5.1. Old Farallon Province (Fast, 800 to 1800+ km Deep)

[37] This vast lower mantle province underlies the east coast of North America, from the Gulf of Mexico to around 45°N, then changes to NW-SE strike across northern Canada. The "Old Farallon" is an extremely robust feature in global tomographies since at least *Grand* [1994] and *van der Hilst et al.* [1997]. It is known to extend deeper than the resolution limits of this regional study, to somewhere between 2000 and 2800 km depth [e.g., *Bijwaard et al.*, 1998; *Montelli et al.*, 2004a; *Simmons et al.*, 2006; *Ren et al.*, 2007; *Li et al.*, 2008], a good synopsis is provided by *Morra et al.* [2010, Figure 3].

[38] The inside-out view of Figure 9 (bottom) highlights the wall-like character of this almost vertically dipping slab. Its young end is truncated rather sharply at 800 km depth and appears decoupled from slab material that immediately succeeded it (the "Laramide Province"). The latter is located clearly further west and spreads out laterally in the *upper* mantle.

[39] The kink or bight between the East Coast and Canadian branches of the Old Farallon was inter-

preted to have been caused by a flat subduction episode and/or break-off of the Kula plate since around 80 Myr [*Bunge and Grand*, 2000; *Ren et al.*, 2007]. Judging by the deep vertical extent of both branches, and by my dating the younger "Laramide Province" to 60–80 Myr (see below), I suggest that this bight must have been in existence significantly before 80 Myr.

5.2. Slow Blanket Above the Old Farallon (Slow, 400 to 1000 km Deep)

[40] This massive band of slow material parallels the east coast of North America at 400 to 1000 km depth and covers the East Coast branch of the Old Farallon from above. It dips oceanward, like the slab underneath (inside-out views of Figures 9 and 10). The slow material is separated from the surface by fast lithosphere (Figure 11) and has no obvious tectonic surface expression. That this slow province presently underlies and parallels the continental margin is presumably a coincidence, since it is located too deep to likely have followed the very mobile lithosphere of North America around over time.

[41] This would suggest a more than coincidental relationship to the slab wall underneath, hence the term "blanket", but I can only speculate about a mechanism. As far as I am aware, only *van der Lee et al.* [2008], using *Grand* [2002], have commented on this slow anomaly, suggesting that it might be an ultradeep dewatering phenomenon. This idea is intriguing in light of increasingly convincing observational evidence that slabs can transport water into the transition zone [e.g., *Kawakatsu and Watada*, 2007; *Cao and Levander*, 2010], and experimental determination of dehydration mechanisms at transition zone depths and below [e.g., *Ohtani*, 2005, and references therein].

[42] However, there is no evidence of a slow blanket above the Old Farallon's Canadian branch. The mantle between the Great Lakes and Hudson Bay is reasonably resolved at 400–1000 km depth (Figure 6), but is not found to be seismically slow (Figures 7 and 8). It seems challenging to explain how one part of the subduction system should produce deep metasomatism but not the other.

[43] The Slow Blanket's deepening toward the Atlantic Ocean appears to be a real effect, in agreement with *van der Lee et al.* [2008] and despite the fact that wave path smearing artifacts are visible at its easternmost limit (yellow, around (35°N, 290°W)). The Slow Blanket may or may nor extend further east. Local deepening of its northern end (55°N, 295°W)

is difficult to evaluate, since structure at these depths should be damped out according to the resolution tests. It is probably not completely artificial, since there is no smearing to the surface, but its real depth extent is uncertain (as is its interpretation).

5.3. Laramide Province (Fast, 300 to 700 km Deep) and the Big Break

[44] The Laramide Province consists of fast material that spreads out laterally and fills the transition zone immediately west of the Old Farallon. Its shallow limit is around 300 km (dark blue in Figure 9, top; also compare Figure 11). The inside-out views reveal a more variable lower limit between 600 and 800 km depth (with exception of a 1100 km deep southern drip (yellow between 32°N, 270°W)). The overall province lacks a clear northeastward dip toward older ages.

[45] Its western limit is a sharp, continental-scale truncation line we termed the "Big Break" (Figure 1), which runs from the Gulf of Mexico into South Dakota around 44°N, 257°W [*Sigloch et al.*, 2008]. Westward of the Big Break, slab is completely absent from the transition zone for several hundred kilometers. Fast material under Kansas/Oklahoma/Texas reaches no deeper than 300 km and appears to represent lithosphere. Hence the Laramide Slab does not connect to the present-day trench. Rather, it marks the finishing line of an abandoned subduction system that comprises the Old Farallon and Laramide provinces.

[46] The termination of the Laramide Province can be dated by comparing the Big Break to the reconstructed trench lines in Figure 1. The trench at 60 Myr coincides with the Old Farallon's young end in the north and south, and also coincides decently with the Big Break at intermediate latitudes. (The mismatch of up to 300 km around 45°N under South Dakota might be accounted for by uncertainty about the exact shape of the continental margin at 60 Myr.) In the big picture, the abandoned subduction system lies east of the 60 Myr trench line, and the currently active system lies west of it.

[47] Assuming the plate broke close to the surface and the flattish Laramide slab sank only vertically (not westward, which seems reasonable), the break must have happened around 60 Myr and not before. Alternatively, a break *at depth* may have happened somewhat *after* 60 Myr. In *Sigloch et al.* [2008], we favored this latter scenario: break around 50 Myr of the shallowly subducting plate after it hit the keel

under stable North America, about 800 km inland of the trench. Subsequently, the remaining 800 km of already-submerged slab would have steepened and rolled back trenchward, leaving a slab-free mantle under present-day Kansas, Oklahoma, and Texas.

[48] The time interval between 80–50 Myr has received intense scrutiny from geologists for its large-scale, anomalous surface observations. These include the extinction of ordinary arc volcanism and onset of the Laramide orogeny, basement-level thrust faulting 500–1000 km inland [e.g., *Dickinson and Snyder*, 1978; *Miller et al.*, 1992; *Humphreys*, 1995]. After 55–45 Myr, thrust faulting terminated and a diffuse westward sweep of volcanism ended in the reestablishment of regular arc volcanism around 35 Myr.

[49] The widely accepted explanation features a segment of the Farallon plate subducting at a very shallow angle, scraping against the lithosphere overhead for hundreds of kilometers eastward [*Humphreys*, 1995; *Saleeby*, 2003]. The imaged geometry indicates that the anomaly termed "Laramide Province" must indeed represent this slab segment. It spreads across the region traversed by the trench between 80 and 60 Myr (Figure 1, bottom) and shows an abrupt termination around the time when thrust faulting ceased. Fifty million years later, it is still hovering subhorizontally at relatively shallow depths, consistent with an initially flat entry angle.

[50] Earlier tomographic models did not have the kind of transition zone resolution required to identify the Laramide Province as a distinct fragment with a distinct history. It should be interesting to assimilate this previously missing slab into mantle convection modeling of North America [e.g., *Bunge and Grand*, 2000; *Liu et al.*, 2008] in order to work out the cause and development of the flat subduction episode.

5.4. The Laramide Province, a Stagnant Slab Under North America

[51] The Laramide slab is lying flat in the transition zone without clear eastward dip (Figure 9, bottom), in marked contrast to the subvertically dipping Old Farallon. This makes it the latest discovery of a "stagnant slab," a subduction style described first and foremost in the western Pacific, where it appears to be quite prevalent (see review by *Fukao et al.* [2009]).

[52] Stagnation on, rather than penetration through, the 660 km discontinuity could be caused by at least three effects: a strong viscosity increase from upper to lower mantle, the endothermic phase transition around 660 km, and a shallow trench entry angle due to trench rollback [*Christensen*, 1996]. Ultra-flat subduction does not seem to be required for triggering the stagnating mode, but presumably would be all the more effective.

[53] Inherent lateral differences in rheology may be harder to defend as a cause, since the North American mantle supported ordinarily steep subduction coeval with the Laramide Province, and also in its wake (the Cascadia system and Anomaly W, see below). This differential behavior has allowed some adjacent, younger slabs to sink hundreds of kilometers into the lower mantle already. Hence I note a significant variability in slab sinking rate, caused by the bistable character of the 660 km discontinuity. Fifty or sixty million years of Laramide stagnation thus represent an observational lower limit on how long a slab can remain in this special mode.

[54] In numerical models [*Christensen*, 1996], the slowing of retrograde trench migration initiates the transition from stagnating to penetrating subduction. The mechanical detachment is located in the transition zone, leaving a subhorizontal fragment behind. Hence a slowing of trench rollback around 60–50 Myr (a time of major global and regional plate reorganization) could have been the cause of the Big Break that ended the Laramide episode.

[55] Tomographic images of the well-instrumented stagnant slab under the Sea of Japan appear to be showing a present-day analogue of the Big Break [*Fukao et al.*, 2009; *Obayashi et al.*, 2010]. Material that enters the north-south-striking Japanese trench dips gently westward, to connect with stagnating material in the transition zone beneath the Sea of Japan and eastern China. The subhorizontal part extends 800–1000 km in plate convergence direction (comparable to 1200 km for the Laramide fragment). However, the young southern and northern ends of the stagnant province appear to show a reinitiation of the penetrating mode. There the slab hits the trench and the 660 km boundary at a very steep angle and has penetrated a few hundred kilometers into the lower mantle already, thus having disconnected from the older subhorizonal piece to the west. If this tearing process migrates south and north toward the center of the province, like a zipper along the 660 km discontinuity that gets unzipped

from both sides, it will create a linear detachment in the transition zone that tracks the location of the trench overhead, a good description of the Big Break at 60 Myr.

6. Mantle Provinces Under Western North America

6.1. Slow Uppermost Mantle Under the Cordillera (Slow, 0 to 400 km Deep)

[56] This low-velocity band is a first-order feature of every body and surface wave tomography: 1000–2000 km wide, it parallels the west coast over at least 5500 km. It is almost pervasive from the surface to 200 km depth, and extends down to 400 km in some places. Its eastern outline coincides rather closely with the eastern limit of the continent's vast topographic high, the North American Cordillera: it strikes north-south through Mexico, Arizona, and Colorado, and changes to NW-SE strike from Wyoming through British Columbia.

[57] The origin and implications of this province, often thought of as synonymous with the "tectonic" West (as opposed to the "stable" East), have been commented on extensively. Body wave resolution is now excellent even close to the surface, thanks to data from the 70 km × 70 km dense grid of USArray broadband stations. Structure in the upper 100 km should not be taken at face value however, since insufficient knowledge of crustal structure can introduce systematic artifacts down to that depth. I apply crustal corrections predicted by model CRUST2.0 [*Bassin et al.*, 2000] and do not allow for free station corrections.

[58] Detailed uppermost mantle anomalies on the scale of the station spacing are resolved beneath the array's footprint, including the thick asthenosphere of the Basin and Range, Snake River Plain, Yellowstone, and most of the Colorado Plateau. Patches of fast structure are found beneath the coast-parallel Cascade and Sierra Ranges, along the recent trench lines (including stuck microplates offshore from southern and Baja California), under northern Idaho and the Columbia Plateau, and the very fast, thick lithosphere under Wyoming (Figure 7). These results are in good agreement with other recent mantle tomographies [e.g., *Burdick et al.*, 2008; *Roth et al.*, 2008; *Tian et al.*, 2009; *Burdick et al.*, 2009; *Tian et al.*, 2011; *Schmandt and Humphreys*, 2010; *Xue and Allen*, 2010; *Obrebski et al.*, 2010; *Lin et al.*, 2008]. In light of my primary focus, the variety of subducted slab geometries underneath, it is perhaps

the large scale, thickness, and relative uniformity of this shallow, slow cover that seems the most remarkable.

[59] The slow anomaly extends at least a few hundred kilometers out into the Pacific and deepens to 800 km. As with its counterpart on the Atlantic side, this deepening of the slow layer under the ocean appears to be largely real, in agreement with *Ren et al.* [2007], even though artificial smearing to depth sets in along its oceanward edge. (The even deeper fast Anomaly X that underlies it is also imaged robustly.)

[60] Only very locally does the slow band extend this deep under the continent. Yellowstone, around 45°N, 250°W is one such case, discussed later. A significantly more prominent deep patch appears under southwestern Canada, yellow/red around 53°N, 240°N. I am not aware of what it might represent or of any surface manifestations.

6.2. Subducted Conjugate of the Mendocino Fracture Zone

[61] Not a seismic province but a subducted paleo-fault, the predicted mirror image ("conjugate") of the Mendocino transform fault on the present-day Pacific seafloor appears as a major underground divide. Not only is the fracture zone itself resolved, as a seismically neutral, east-west striking, narrow divide between two fast slab segments to the north and south. The depth of slab segments also differs greatly across this line: transition zone slab to the north (Figure 9, top, dark blue "Cascadia Province" under Nevada/Utah/Colorado), versus lower mantle slab to the south (green-yellow "Anomaly W" under Arizona and New Mexico). The imaged length of this subducted fracture zone, from Cape Mendocino to (37°N, 255°W), is 1700 km.

[62] The transition zone slab to the north represents ongoing subduction of the Juan de Fuca (Farallon) plate, whose southern boundary delineates the Mendocino Conjugate from the Mendocino triple junction through Nevada. Further east, the subducted fault straddles the state borders of Utah/Colorado and Arizona/New Mexico, and is defined by northern and southern slabs jointly. At least for the past 20 Myr, the fault's observed location agrees well with predictions from tectonic reconstructions (Figure 1) [also *Engebretson et al.*, 1985; *Schmid et al.*, 2002].

[63] Note another example of differential sinking: the vertical offset of several hundred kilometers across the Mendocino Conjugate, of material that

must have subducted at the same time and was nominally part of the same plate, implies that the fault allowed for significant mechanical decoupling. Interestingly, *Atwater* [1989] predicted from a kink and a zigzag band in the magnetic stripes on the Pacific plate that such decoupling could have started as early as 55 Myr (the time of the Big Break), 25 Myr before the slab window beneath California actually opened. This longer time span would match the large vertical offset that has accumulated to present.

[64] Segmentation of a sheet-like slab into narrower slivers, such as here, significantly modifies the subduction dynamics [*Wortel and Spakman*, 2000; *Schellart*, 2005; *Schellart et al.*, 2007]. Ambient mantle can flow in through the slab tears, for example allowing individual trench segments to roll back more easily.

6.3. Anomaly W (Fast, 800 to 1300 km Depth): Post-Laramide Subduction South of the Mendocino Fracture Zone

[65] Here I consider subducted material south of the Mendocino Conjugate Fracture, and west of the Big Break (i.e., more recent than 50 or 60 Myr). Under Texas/Oklahoma/Kansas, fast material is present only to 300 km depth, which I interpret as purely lithospheric (Figure 9, bottom). Such thick cratonic lithosphere is consistent with surface wave evidence [e.g., *Nettles and Dziewonski*, 2008]. Further west, fast lower mantle Anomaly W is located at 800–1300 km depth under New Mexico and Arizona. It must represent the terminal stage of Farallon subduction south of the Mendocino, before and while the Pacific plate made contact with North America. The first contact around 30 Myr was followed by a gradual opening and extension of a slab-free window under almost all of California (best seen in Figure 11, top left), as the Pacific-Farallon ridge south of the Mendocino Conjugate subducted.

[66] The upper mantle south of the Mendocino Conjugate is slab-free. From above, Anomaly W is covered by slow material (400 km thick asthenosphere under the southern Basin and Range), and by neutral material in the transition zone. Other recent regional models seem to agree with this upper mantle assessment [*Burdick et al.*, 2009; *Tian et al.*, 2009; *Schmandt and Humphreys*, 2010], and a recent global model confirms the presence of Anomaly W [*Li et al.*, 2008] (at 1050 km depth).

[67] Slab W seems to have sunken through the 660 km discontinuity without delay and at fairly steep angle, evidenced by its deep location as compared to the coeval Cascadia slab foundering in the transition zone, just north of the Mendocino Conjugate.

[68] The Big Break strikes in NNW-SSE direction, whereas the slabs west of it, Anomaly W and the Cascadia system, line up in north-south direction. It is this clockwise rotation in subduction strike that leaves the mantle under Texas slab-free *at all depths*. There are two obvious alternatives for generating such a slab-free sector, as follows.

[69] 1. Material kept entering the trench immediately after the Big Break, but subsequently migrated westward across the mantle that is now underlying Texas (option 1). This requires *lateral material displacement inside the mantle* over hundreds of kilometers, and hence a clear deviation from vertical sinking.

[70] 2. Subduction effectively ceased while the system was rotating itself into north-south direction after the Big Break (option 2). The trench was not or hardly being fed with slab while it rolled across the Texan mantle, but picked up again later with the subduction of Anomaly W. The vertical sinking assumption would not be violated. One possible cause for a temporary hiatus in subduction is the accretion of an oceanic terrane.

[71] In the bigger picture, determining the causes of slab-free mantle columns is relevant because western North America has a complicated history of terrane accretion. Still incompletely understood, this knowledge is based on land geology, and is not adequately reflected in the geometries of (seafloor-based) plate reconstructions if the magnetic stripes were subducted. Slab fragments offer a second line of evidence to complement the study of accreted terranes [e.g., *van der Meer et al.*, 2010]. However, this method of inference will work only to the extent that subducted slabs do not move over arbitrary lateral distances, which would obscure their origin and timing. Hence it would be interesting to rule out option 1.

[72] In favor of option 1, none of the oceanic plate reconstructions showed a hiatus in convergence during the 10–20 Myr following the Big Break. However, this was an interval of major plate reorientation in the Pacific Basin, so that convergence velocities and directions come with considerable uncertainties [*Engebretson et al.*, 1985; D. Müller, personal communication, 2010].

[73] The weakness of option 1 is an apparent lack of driving forces to generate large lateral displacement

of slab fragments, whereas vertical sinking is clearly driven by gravity. Predominantly vertical particle sinking is also consistent with the observed retrograde migration of the Farallon trench, the rigid upper mantle slab pushing the trench oceanward as it settled [*Goes et al.*, 2008]. Note that large-scale lateral movement is *not* needed to explain the kind of "slab rollback" inferred from westward migration of volcanism in the wake of the Laramide episode ("ignimbrite sweep") [e.g., *Humphreys*, 1995]. In order to replace an ultraflat slab with inflowing fertile asthenosphere, it suffices for the (already fragmented) slab to sink vertically by a couple hundred kilometers. Even if not perfectly vertical, such sinking would not generate a slab-free region many hundred kilometers wide.

6.4. Cascadia, the Currently Active Subduction System (Fast, 0 to 1800+ km Depth)

[74] The Cascadian subduction system is the most massive slab pile that accumulated anywhere under North America in the past 60+ Myr. I am referring to fast material that extends from north of the Mendocino Conjugate line into southwestern Canada, and choose the name "Cascadia" because the youngest part of this slab connects upward to the present-day trench along the Cascade Ranges. Geometrically, this is undoubtedly the most complex three-dimensional geometry of all mantle provinces discussed. It extends continuously across all imaged depth levels, from the surface to at least 1800 km depth.

6.4.1. Uppermost Mantle

[75] The uppermost 400 km contain recently subducted slab under northern California, Oregon, and Washington (Figure 11, top left). The slab appears heavily fragmented close to the trench, a trait shared by all recent tomographies [*Burdick et al.*, 2008; *Roth et al.*, 2008; *Burdick et al.*, 2009; *Tian et al.*, 2009, 2011; *Schmandt and Humphreys*, 2010; *Xue and Allen*, 2010; *Obrebski et al.*, 2010]. Presumably this reflects the breakup and rotation over the past 5–10 Myr of the Juan de Fuca plate into three microplates, although *Roth et al.* [2008] state that even a truly continuous slab would appear fragmented, due to imperfect seismic illumination.

6.4.2. Transition Zone

[76] In the transition zone, the subducted material flattens out and thickens to fill most or all of the transition zone (Figure 9, top). I regard this as a second example of the stagnating mode. The slab is divided by a SW-NE trending plate tear (the Slab Gap). The southern transition zone segment has triangular shape and extends between Mendocino Conjugate Fracture, Snake River Plain, and 250°W. This segment, termed "S1" by *Sigloch et al.* [2008], has been more aptly called the Gorda slab by *Cao and Levander* [2010], since it connects upward to the remaining sliver of Gorda microplate seafloor. They find that it creates a depression on the 660 km discontinuity strong enough that slab dehydration processes must be invoked. The Gorda slab is covered by very slow, 300+ km thick asthenosphere, an anomaly that intensifies toward Yellowstone. The hot spot is located above the northeastern corner of the Gorda slab, and its track is underlain by the stagnating slab.

[77] The northern slab segment could be called the Juan de Fuca plate proper (termed "N1" by *Sigloch et al.* [2008]). Its geometry is even more complex, apparently involving a slab that dips into the lower mantle at a normally steep angle, but is partly overlain by a stagnating fragment at its northern edge (just north of the U.S.-Canadian border, between 240°W and 260°W). The asthenosphere above the Juan de Fuca slab is interspersed with additional, smaller fragments of fast material, just south of the U.S.-Canadian border.

6.4.3. The Slab Gap, a Major Divide

[78] The Slab Gap marks a division line between upper mantle fragments (N1 and S1), but it reaches much deeper. It is a major, SW-NE trending fracture in the Cascadia system, striking from near the trench under southern Oregon into the lower mantle under the U.S.-Canadian border around 255°W. Projected to the surface, the length of the Slab Gap is around 1800 km. The tear seems to heal and disappear below 1100 km depth (e.g., Figure 3, right). However, at transition zone depths its strike continues further to the northeast for another 700 km, as northern limit of the Laramide Province.

[79] Presumably the Slab Gap is as old as the slab at 1100 km depth, and/or as old as the Laramide Province (i.e., older than 50 Myr). It must be a passive break in the plate, since its sides have not diverged nor closed over this whole time. I take this as observational evidence for almost vertical sinking, since large-scale lateral displacement would likely also have generated some differential shifting, so that the narrow, linear break geometries of

Interprets the YS-SRP as a slab gap

Slab Gap and Mendocino Conjugate would not have been preserved for tens of millions of years.

[80] In the upper mantle and transition zone, the Slab Gap seems to mark the northern limit of the Gorda microplate, implying that this long-lived underground feature directly relates to the recent (5–10 Myr) fracturing of the Juan de Fuca plate. The old age of the tear implies that the plume head presumed to have generated the Columbia River flood basalts around 17 Myr would have been free to ascend through it. It means that there was no need for the plume to have burned a hole in the plate and displaced large volumes of slab, as suggested by *Xue and Allen* [2010] and *Obrebski et al.* [2010]. The Slab Gap widens under Montana, the mantle region that was underlying the Columbia Plateau 17 Myr ago.

chicken and egg argument - was the tear there first or was the plume there first

[81] This fracture or tear was first identified by *Sigloch et al.* [2008]. As a thin, seismically neutral feature sandwiched between two fast slabs, a plate tear is a delicate imaging target. It is nonetheless well resolved. Nothing about its geometry or about the resolution tests suggests imaging artifacts. This testifies to the quality of USArray data and the finite-frequency modeling, which is particularly good at detecting small-scale structure at depth. The multi-frequency *S* wave studies by *Tian et al.* [2009, 2011] have confirmed the Slab Gap.

6.4.4. Cascadia Root in the Lower Mantle

[82] In the lower mantle, the Cascadia system sank to at least 1800 km depth. Its deep "root" below 1200 km is the most massive part of the system, dominating the lower mantle under the midcontinent (blue dashed outline in Figure 1, and the red/pink material in Figure 9, bottom). The Cascadia Root strikes NW-SE and stretches for about 2000 km, roughly from 50°N, 240°W to 40°N, 265°W.

[83] From 1200 km upward, there is a transition to a more fragmented regime. The upward connection narrows and the slab splits into two "pillars", divided by the SW-NE striking Slab Gap (best seen in Figure 12, first column). Above 900 km, the northern pillar (under Alberta/Saskatchewan/Montana) stays intact and continuous into the upper mantle, whereas the southern one fragments (Figure 12, top left). Its geometrical continuation in the upper mantle is clearly the Gorda Slab, but the two slabs are barely connected across the 670 km discontinuity (Figure 11, bottom left). This also seems to reflect the clockwise rotation of

the whole Cascadia system after the Big Break. The rotation hinge must have been close to the northern pillar, whereas the southern pillar was sheared off by the rotation.

[84] I am not aware that the lower mantle Cascadia Root had been discussed prior to *Sigloch et al.* [2008], even though a check of recent global tomography models confirms its presence [*Bijwaard et al.*, 1998; *Montelli et al.*, 2004a; *Ren et al.*, 2007; *Li et al.*, 2008; *Amaru*, 2007]. Perhaps it was not discussed earlier because resolution seemed questionable and/or the presence of a slab in this midcontinent location did not make sense, especially not beneath Yellowstone, the location of a presumed mantle plume.

[85] In their global survey of lower mantle slabs, *van der Meer et al.* [2010] have since interpreted it as having being generated from 186 Myr to 92 Myr (their "Idaho slab"), but they did not consider or explain its continuous upward connection to the present-day Cascadia trench, which was pointed out by *Sigloch et al.* [2008]. The observation that the Cascadia Root is not an isolated lower mantle feature, but rather the old end of the currently active subduction, adds strong geometrical and timing constraints on its interpretation.

6.4.5. Yellowstone (Slow, 0 to 900 km Deep)

[86] Yellowstone as a mantle province does not jump out on a scale comparable to the vast slab assemblages in Figure 1. It manifests itself as the intensely slow and thick asthenosphere of the Snake River Plain discussed earlier, and as a slow, potato-shaped midmantle anomaly at 500–900 km depth, centered on 45°N, 250°W in Figure 10, bottom. Its maximum lateral width is 500 km, at depths of 600–700 km. The slow anomaly is surrounded by fragments of fast material: it emerges from within the Cascadian slab pile (Figures 7 and 8). A follow-up paper will be devoted specifically to the mantle under Yellowstone.

6.5. Interpretation of Cascadia Subduction: An Oceanic Arc Turned Continental

[87] The most striking and puzzling aspect about Cascadia is that its root seemingly lies too deep for its westerly location. In depth extent and sheer volume, the lower mantle Cascadia Root is fully comparable to the Old Farallon itself, but it is located west of the 60 Myr Farallon trench line. Plate reconstructions of the Farallon trench account for the Old Farallon and Laramide slabs, but there

is no additional, more westerly trench that would separately account for the Cascadia Root. But it is not clear that a time span of 80 Myr since subduction (into the Farallon trench) would have sufficed to bring the Cascadia Root to its current depth and location.

[88] From their visual similarity in the inside-out view of Figure 9, an unbiased observer would probably guess that the Cascadia Root subducted over the same time interval and in much the same style as the Old Farallon, and hence into a different trench. I will make the case that this may actually be true. It would imply that the Cascadia Root had already been subducting into an intraoceanic trench for tens of millions of years, and kept subducting while and after that trench was swept up by the westward moving continent. At that time, Cascadia subduction would have morphed into the continental arc that it is today. In effect, we need to evaluate two competing hypotheses, as follows.

[89] 1. The plate reconstructions are complete, the only trench in existence was the Farallon trench along the continental margin. The Cascadia Root subducted into this trench *after* the Old Farallon and/or Laramide slabs had finished subducting.

[90] 2. The Cascadia Root subducted into a more westerly, intraoceanic trench (not present in the plate constructions), at the same time as the Old Farallon and Laramide slabs were subducting into the continental Farallon trench. At some point, the oceanic trench must have become the present-day, continental trench, because the deep Cascadia Root unambiguously connects upward to slab currently entering the Cascadia margin. The ocean arc (plus any terranes it had swept up) accreted to North America. The old continental Farallon trench shut off around that time; I make an argument that it was around 50–60 Myr.

[91] Scenario 1 is essentially what was suggested by *Sigloch et al.* [2008], and it still works for the slabs south of the Mendocino Conjugate line. But it appears that the slab inventory of the Cascadia system cannot be reasonably accounted for in this way, and that the solution of an additional trench is more satisfying. From a land geologist's point of view, the idea would seem natural, since accreted terranes are a matter of fact. Note that the deepest Cascadia Root is crescent-shaped in the tomographic image, as might be expected from a northeastward subducting ocean arc (Figure 9, inside-out view).

[92] The problem with scenario 1 is that the Cascadia Root had to sink much faster than the Old

Farallon, in order for the two slabs to have similar appearance today. In addition, this massive slab would have experienced large lateral displacement toward the southwest. A relatively confident subduction age estimate of 80 Myr can be assigned to the shallow, *young* end of the Old Farallon, located at 800–900 km depth (yellowish green truncation in Figure 9, top). Trench reconstructions and the location of its successor, the Laramide slab, both point to this age. All deeper material is older. The Old Farallon is a very steep and massive slab, and was probably not particularly slow to sink, since areas of abundant subduction are associated with fast sinking [*Steinberger*, 2000; *Goes et al.*, 2008]. In scenario 1, the Cascadia Root could not have subducted longer than 80 Myr ago, so it would have sunk to at least 1800 km depth within this time, whereas the Old Farallon of this age is still located around 900 km.

[93] In another line of problematic evidence, sinking rates in the lower mantle are estimated between 1–2 cm/yr [*Grand*, 1994; *Steinberger*, 2000; *Goes et al.*, 2008; *van der Meer et al.*, 2010]. In probably the most comprehensive survey, *van der Meer et al.* [2010] argue that 1.2 cm/yr fits sinking slabs globally. Cascadia would have needed to sink 2.25 cm/yr (1800 km in 80 Myr).

[94] An even more serious problem is the large lateral displacement inside the mantle required of the entire Cascadia Root, should it really have subducted into the Canadian Branch of Old Farallon. The distance between Old Farallon and Cascadia Root is more than 1000 km, measured perpendicularly to the two slabs in the lower mantle. The massive Cascadia Root could not have moved laterally by 1000 km in an upper mantle that is only 670 km thick. In the much more viscous lower mantle, with the slab mechanically disconnected from the trench, there is no force to drive lateral displacement. I conclude that making the Cascadia Root sink obliquely and fast enough after subduction into the Farallon trench is a very unlikely proposition.

[95] In scenario 2, the Cascadia Root was subducting eastward into an oceanic trench, contemporaneous with the Old Farallon, and its material sank more or less vertically after entering the trench. The trench itself did not migrate much either, since the Cascadia Root is a steep slab that shows no clear tilt. The oceanic arc terrane, and any other terranes this system had accumulated, accreted to North America when the Farallon trench swept across the (former and current) location of the Cascadia Root. This happened

So it could help explain the Siletzia story a little better, but are these large high velocities really slabs?

around 60–50 Myr, according to Figure 1. It should have been the most recent accretion event in this region, since the Cascadia slab system shows no signs of disruption or hiatus since.

[96] This prediction appears to fit the geological record: according to *Dickinson* [2004, Figure 1], the latest accretion event involved a massive terrane called Siletzia, at around 50 Myr. Hence Siletzia should be the terrane package associated with Cascadia Root subduction. Before Siletzia accreted, Farallon subduction had a NW-SE strike ("Challis-Absaroka arc"), due to a large embayment in the continent's west coast [*Dickinson*, 2004, Figure 8; *Humphreys*, 2009, Figure 2]. This matches the NW-SE strike of the Old Farallon's Canada Branch. Siletzia supposedly accreted with this same strike (matching the strike of the Cascadia Root). Subduction into the Old Farallon trench ceased. There is a nearly slab-free zone between the Canada Branch and Cascade Root (under Manitoba and Saskatchewan) to reflect the expected hiatus during accretion and trench jump. The Siletzia terranes filled up the Columbia embayment, smoothing out the shape of the coastline. This deformation of the trench would have been the time when the Cascadia slab split into two pillars, narrowed and deformed. The oceanic trench had become a continental trench and started to roll back with the continent; the corresponding slab pile shows a clear westward tilt from 1000 km depth upward. In the course of Basin and Range extension, the accreted terranes underwent a clockwise rotation of about 50° [*Dickinson*, 2004, Figure 8; *Humphreys*, 2009, Figure 2]. This matches the rotation of the entire subduction system, as inferred from the slab-free sector between the Big Break and Anomaly W, and the north-south strike of more recently subducted slabs.

[97] The underground geometry fits the geological record to considerable detail. No dynamically unlikely slab movements are required. Hence this solution of an oceanic-turned-continental arc for Cascadia seems more satisfying to me. The suggestion that Siletzia should be tomographically visible is due to *Schmandt and Humphreys* [2010], although they focus on a much smaller upper mantle anomaly under Idaho and Oregon as possibly the leading edge of Siletzia.

[98] Note that midmantle anomalies K (offshore British Columbia, fast, 900 to 1300+ km) and X (offshore California, fast, 900 to 1500+ km) likely represent other episodes of intraoceanic subduction. Anomaly K is also present in other models

[e.g., *Bijwaard et al.*, 1998; *Montelli et al.*, 2004a; *Ren et al.*, 2007; *Li et al.*, 2008; *Amaru*, 2007], and has been interpreted as Kula plate by *Ren et al.* [2007].

7. Synopsis

[99] Summing up this inventory of mantle provinces, I was able to provide a reasonably coherent account, spatially and temporally, of large-scale seismic anomalies in the upper and middle mantle under the North American continent. Some of them had not been discussed much in the literature: the Slow Blanket overlying the Old Farallon, the transition zone Laramide slab, the deep root of Cascadia, and the lower mantle fragment W.

[100] The first-order division at the surface between stable East and tectonic West is shown to have its equivalent in the mantle: slabs that were laid down before or after (east or west of) the Big Break around 50–60 Myr. A key position in the analysis is occupied by the newly imaged "Laramide" province, a stagnant slab analogous to the subhorizontal transition zone slabs in the Western Pacific and Mediterranean. The Laramide Province provides a robust, dateable anchor halfway through the 150+ million years of Farallon subduction history, thanks to the convergence of three independent lines of evidence:

[101] 1. For the time between 80 Myr and 60 (or 50) Myr, a time of rapid plate convergence, land geologists have inferred anomalously flat subduction under North America.

[102] 2. I image a 1200 km wide stagnating slab in the region in question. Subhorizontal stagnation in the transition zone is known to be linked to flat trench entry angle.

[103] 3. Trench reconstructions map the beginning and end of the stagnant piece to 80 Myr and 60 Myr, respectively. This closes the circle of reasoning. (Note that using paleotrench positions to establish timing works best on slabs that spread out horizontally, like this one.)

[104] The other new key element is the deep root of Cascadia subduction. Comparison to the paleotrenches indicates either a huge deviation from vertical sinking, or that an (intraoceanic) trench is missing from the plate reconstructions. I conclude that the latter is more likely, since it also seems to be supported by the geological record. In this way, the reconciliation of tomogra-

phy and plate reconstructions can serve as a real tool for discovery.

8. Conclusion

[105] The mantle under North America has evidently supported a wide variety of subduction behaviors, something geologists had inferred indirectly from the surface geological record. Now the high-resolution tomographic images enabled by USArray allow for detailed structural examination of the slabs that caused the upheavals at the surface. Suitable three-dimensional visualization plays an important role, e.g., in the form of "color-banded 3-D maps" developed here.

[106] The recognition of the lower mantle slab pile under the northwestern United States as former intraoceanic subduction associated with the Siletzia terrane is new, as far as I know. The discovery of the previously "missing" Laramide province implies that mantle anomalies under eastern North America are older than has been assumed in some interpretations [e.g., *Bunge and Grand*, 2000; *Ren et al.*, 2007]. For example, the prominent bight or bend on the Old Farallon system cannot have been caused by the Kula break around 80 Myr, since it clearly predates the flat episode, which started around 80–90 Myr. It follows that Farallon fragments in the lowermost mantle are almost certainly older than the 120 Myr estimated by *Ren et al.* [2007] (who use *Steinberger* [2000]) and by *Bunge and Grand* [2000]. It is good news if more surface history is still being held in memory by the convecting mantle system.

[107] The different depths of the Laramide province versus Cascadia and Anomaly W provide stark examples of variable sinking rates of adjacent slab fragments. The reason is that not all fragments transition seamlessly through the upper-lower mantle boundary. This serves a note of caution against a common default assumption in interpreting slab fragments, namely that slabs sink evenly, and that therefore a fixed depth corresponds to a fixed age [e.g., *Ren et al.*, 2007; *van der Meer et al.*, 2010]. In the case of the stagnating province, the slab has been delayed for more than 50 Myr already. The bistable character of the 660 km discontinuity, which lets some fragments pass but not others, must somehow reflect surface input conditions [e.g., *Goes et al.*, 2008], thus generating a mantle system with a richer set of behaviors. This complicates province interpretation but also implies more interesting, truly four-dimensional connections than does uniform sinking.

References

Akcelik, V., J. Bielak, and O. Ghattas (2007), Full waveform inversion for seismic velocity and anelastic losses in heterogeneous structures, *Bull. Seismol. Soc. Am.*, *97*(6), 1990–2008, doi:10.1785/0120070079.

Amaru, M. (2007), Global travel time tomography with 3-D reference models, Ph.D. thesis, Utrecht Univ., Utrecht, Netherlands.

Atwater, T. (1989), Plate tectonic history of the northeast Pacific and western North America, in *The Eastern Pacific Ocean and Hawaii (The Geology of North America)*, edited by E. L. Winterer, D. M. Hussong, and R. W. Decker, pp. 21–72, Geological Soc. of Am., Boulder, Colo.

Bassin, C., G. Laske, and G. Masters (2000), The current limits of resolution for surface wave tomography in North America, *EosTrans. AGU*, *81*(48), Fall Meet. Suppl., Abstract F897.

Bijwaard, H., W. Spakman, and E. Engdahl (1998), Closing the gap between regional and global travel time tomography, *J. Geophys. Res.*, *103*, 30,055–30,078.

Bostock, M. G., and J. C. VanDecar (1995), Upper-mantle structure of the northern Cascadia subduction zone, *Can. J. Earth Sci.*, *32*, 1–12.

Boyden, J., R. Müller, M. Gurnis, T. Torsvik, J. Clark, M. Turner, H. Ivey-Law, J. Farrow, and R. Watson (2011), Next-generation plate-tectonic reconstructions using GPlates, in *Geoinformatics: Cyberinfrastructure for the Solid Earth Sciences*, edited by G. Keller and C. Baru, Cambridge Univ. Press, Cambridge, U. K., in press.

Bunge, H.-P., and S. Grand (2000), Mesozoic plate-motion history below the northeast Pacific Ocean from seismic images of the subducted Farallon slab, *Nature*, *405*, 337–340.

Burdick, S., et al. (2008), Upper mantle heterogeneity beneath North America from travel time tomography with global and USArray transportable array data, *Seismol. Res. Lett.*, *79*(3), 384–392.

Burdick, S., R. van der Hilst, F. Vernon, V. Martynov, T. Cox, J. Eakins, T. Mulder, L. Astiz, and G. Pavlis (2009), Model update December 2008: Upper mantle heterogeneity beneath North America from *P* wave travel time tomography with global and USArray transportable array data, *Seismol. Res. Lett.*, *80*(4), 638–645.

Cao, A., and A. Levander (2010), High-resolution transition zone structures of the Gorda Slab beneath the western United States: Implication for deep water subduction, *J. Geophys. Res.*, *115*, B07301, doi:10.1029/2009JB006876.

Christensen, U. R. (1996), The influence of trench migration on slab penetration into the lower mantle, *Earth Planet. Sci. Lett.*, *140*, 27–39, doi:10.1016/0012-821X(96)00023-4.

Dahlen, F. A. (2005), Finite-frequency sensitivity kernels for boundary topography perturbations, *Geophys. J. Int.*, *162*, 525–540, doi:10.1111/j.1365-246X.2005.02682.x.

Dahlen, F., and A. Baig (2002), Fréchet kernels for body wave amplitudes, *Geophys. J. Int.*, *150*, 440–466.

Dahlen, F., S. Hung, and G. Nolet (2000), Fréchet kernels for finite-frequency travel-times-i. Theory, *Geophys. J. Int.*, *141*, 157–174.

Dickinson, W. (2004), Evolution of the North American Cordillera, *Annu. Rev. Earth Planet. Sci.*, *32*, 13–45, doi:10.1146/annurev.earth.32.101802.120257.

Dickinson, W., and W. Snyder (1978), Plate tectonics of the Laramide Orogeny, in *Laramide Folding Associated With Basement Block Faulting in the Western United States*, edited by V. Matthews, *Mem. Geol. Soc. Am.*, 151, 355–366.

Engebretson, D., A. Cox, and R. Gordon (1985), Relative motions between oceanic and continental plates in the Pacific Basin, *Spec. Pap. Geol. Soc. Am.*, *206*,.

Fichtner, A., H. Igel, H.-P. Bunge, and B. L. N. Kennett (2009), Simulation and inversion of seismic wave propagation on continental scales based on a spectral-element method, *J. Numer. Anal. Ind. Appl. Math.*, *4*(1–2), 11–22.

Fukao, Y., M. Obayashi, and T. Nakakuki (2009), Stagnant slab: A Review, *Annu. Rev. Earth Planet. Sci.*, *37*, 19–46, doi:10.1146/annurev.earth.36.031207.124224.

Goes, S., F. Capitanio, and G. Morra (2008), Evidence of lower-mantle slab penetration phases in plate motions, *Nature*, *451*, 981–984, doi:10.1038/nature06691.

Grand, S. (1994), Mantle shear structure beneath the Americas and surrounding oceans, *J. Geophys. Res.*, *99*, 11,591–11,621.

Grand, S. (2002), Mantle shear-wave tomography and the fate of subducted slabs, *Philos. Trans. R. Soc. London A*, *360*, 2475–2491, doi:10.1098/rsta.2002.1077.

Harris, R. A., H. M. Iyer, and P. B. Dawson (1991), Imaging the Juan de Fuca Plate beneath southern Oregon using teleseismic *P* wave residuals, *J. Geophys. Res.*, *96*, 19,879–19,889.

Humphreys, E. (1995), Post-Laramide removal of the Farallon slab, western United States, *Geology*, *23*, 987–990.

Humphreys, E. (2009), Relation of flat subduction to magmatism and deformation in the western United States, in *Backbone of the Americas*, edited by S. Kay, V. Ramos, and W. Dickinson, *Mem. Geol. Soc. Am.*, 204, 85–98, doi:10.1130/2009.1204(04).

Hung, S., F. Dahlen, and G. Nolet (2000), Fréchet kernels for finite-frequency travel-times-ii. Examples, *Geophys. J. Int.*, *141*, 175–203.

Hung, S.-H., Y. Shen, and L.-Y. Chiao (2004), Imaging seismic velocity beneath the Iceland hot spot: A finite-frequency approach, *J. Geophys. Res.*, *109*, B08305, doi:10.1029/2003JB002889.

Jahnke, G., M. Thorne, A. Cochard, and H. Igel (2008), Global *SH* wave propagation using a parallel axisymmetric spherical finite-difference scheme: Application to whole mantle scattering, *Geophys. J. Int.*, *173*, 815–826, doi:10.1111/j.1365-246X.2008.03744.x.

Käser, M., and M. Dumbser (2006), An arbitrary high order discontinuous Galerkin method for elastic waves on unstructured meshes I: The two-dimensional isotropic case with external source terms, *Geophys. J. Int.*, *166*, 855–877, doi:10.1111/j.1365-246X.2006.03051.x.

Kawakatsu, H., and S. Watada (2007), Seismic evidence for deep-water transportation in the mantle, *Science*, *316*, 1468–1471, doi:10.1126/science.1140855.

Kennett, B., and E. Engdahl (1991), Traveltimes for global earthquake location and phase identification, *Geophys. J. Int.*, *105*, 429–465.

Komatitsch, D., and J. Tromp (1999), Introduction to the spectral-element method for 3-D seismic wave propagation, *Geophys. J. Int.*, *139*, 806–822.

Li, C., R. D. van der Hilst, E. R. Engdahl, and S. Burdick (2008), A new global model for *P* wave speed variations in Earth's mantle, *Geochem. Geophys. Geosyst.*, *9*, Q05018, doi:10.1029/2007GC001806.

Lin, F.-C., M. Moschetti, and M. Ritzwoller (2008), Surface wave tomography of the western United States from ambient seismic noise: Rayleigh and Love wave phase velocity maps, *Geophys. J. Int.*, *173*, 281–298, doi:10.1111/j.1365-246X.2008.03720.x.

Liu, L., S. Spasojevic, and M. Gurnis (2008), Reconstructing Farallon plate subduction beneath North America back to the Late Cretaceous, *Science*, *322*(5903), 934–938, doi:10.1126/science.1162921.

Miller, D., T. Nilsen, and W. Bilodeau (1992), Late Cretaceous to early Eocene geologic evolution of the U.S. Cordillera, in *The Cordilleran Orogen: Conterminous U.S.*, edited by B. Burchfiel et al., p. 205–260, Geological Soc. of Am., Boulder, Colo.

Montelli, R., G. Nolet, F. Dahlen, G. Masters, E. Engdahl, and S.-H. Hung (2004a), Global *P* and *PP* travel time tomography: Rays vs. waves, *Geophys. J. Int.*, *158*, 637–654.

Montelli, R., G. Nolet, D. F. A., G. Masters, E. Engdahl, and S.-H. Hung (2004b), Finite-frequency tomography reveals a variety of plumes in the mantle, *Science*, *303*, 338–343.

Morra, G., D. Yuen, L. Boschi, P. Chatelain, P. Koumoutsakos, and P. Tackley (2010), The fate of the slabs interacting with a viscosity hill in mid-mantle, *Phys. Earth Planet. Inter.*, *180*, 271–282.

Müller, R., J.-Y. Royer, and L. Lawver (1993), Revised plate motions relative to the hotspots from combined Atlantic and Indian Ocean hotspot tracks, *Geology*, *21*, 275–278.

Nettles, M., and A. Dziewonski (2008), Radially anisotropic shear-velocity structure of the upper mantle beneath North America, *J. Geophys. Res.*, *113*, B02303, doi:10.1029/2006JB004819.

Nissen-Meyer, T., A. Fournier, and F. A. Dahlen (2007), A 2-D spectral-element method for computing spherical-earth seismograms-I. Moment-tensor source, *Geophys. J. Int.*, *168*, 1067–1093.

Obayashi, M., et al. (2010), Transition from slab stagnation to penetration, paper presented at Japan Geoscience Union Meeting, Chiba, Japan.

Obrebski, M., R. M. Allen, M. Xue, and S. Hung (2010), Slab-plume interaction beneath the Pacific Northwest, *Geophys. Res. Lett.*, *37*, L14305, doi:10.1029/2010GL043489.

Ohtani, E. (2005), Water in the mantle, *Elements*, *1*(1), 25–30.

O'Neill, C., D. Müller, and B. Steinberger (2005), On the uncertainties in hot spot reconstructions and the significance of moving hot spot reference frames, *Geochem. Geophys. Geosyst.*, *6*, Q04003, doi:10.1029/2004GC000784.

Persson, P.-O., and G. Strang (2004), A simple mesh generator in MATLAB, *SIAM Rev.*, *46*(2), 329–345.

Rasmussen, J., and E. Humphreys (1988), Tomographic image of the Juan de Fuca plate beneath Washington and western Oregon using teleseismic *P* wave travel-times, *Geophys. Res. Lett.*, *15*, 1417–1420.

Ren, Y., E. Stutzman, R. D. van der Hilst, and J. Besse (2007), Understanding seismic heterogeneities in the lower mantle beneath the Americas from seismic tomography and plate tectonic history, *J. Geophys. Res.*, *112*, B01302, doi:10.1029/2005JB004154.

Ritsema, J., H. J. van Heijst, J. H. Woodhouse, and A. Deuss (2009), Long-period body wave traveltimes through the crust: implication for crustal corrections and seismic tomography, *Geophys. J. Int.*, *179*, 1255–1261, doi:10.1111/j.1365-246X.2009.04365.x.

Roth, J. B., M. J. Fouch, D. E. James, and R. W. Carlson (2008), Three-dimensional seismic velocity structure of the northwestern United States, *Geophys. Res. Lett.*, *35*, L15304, doi:10.1029/2008GL034669.

Saleeby, J. (2003), Segmentation of the Laramide Slab-Evidence from the southern Sierra Nevada region, *Geol. Soc. Am. Bull.*, *115*, 655, doi:10.1130/0016-7606.

Schellart, W. (2005), Influence of the subducting plate velocity on the geometry of the slab and migration of the subducting hinge, *Phys. Earth Planet. Inter.*, *231*, 197–219.

Schellart, W., J. Freeman, D. Stegman, L. Moresi, and D. May (2007), Evolution and diversity of subduction zones controlled by slab width, *Nature*, *446*, 308–311.

Schmandt, B., and E. Humphreys (2010), Complex subduction and small-scale convection revealed by body-wave tomography of the western United States upper mantle, *Earth Planet. Sci. Lett.*, *297*, 435–445, doi:10.1016/j.epsl.2010.06.047.

Schmid, C., S. Goes, S. van der Lee, and D. Giardini (2002), Fate of the Cenozoic Farallon slab from a comparison of kinematic thermal modeling with tomographic images, *Earth Planet. Sci. Lett.*, *204*, 17–32, doi:10.1016/S0012-821X(02)00985-8.

Schuberth, B., H. Bunge, G. Steinle-Neumann, C. Moder, and J. Oeser (2009), Thermal versus elastic heterogeneity in high-resolution mantle circulation models with pyrolite composition: High plume excess temperatures in the lowermost mantle, *Geochem. Geophys. Geosyst.*, *10*, Q01W01, doi:10.1029/2008GC002235.

Sigloch, K. (2008), Multiple-frequency body-wave tomography, Ph.D. thesis, Princeton Univ., Princeton, N. J.

Sigloch, K., and G. Nolet (2006), Measuring finite-frequency body wave amplitudes and traveltimes, *Geophys. J. Int.*, *167*, 271–287, doi:10.1111/j.1365-246X.2006.03116.x.

Sigloch, K., and G. Nolet (2008), Joint multifrequency inversion of teleseismic *P* wave amplitudes and traveltimes for 3-D velocity and attenuation structure under North America, *Eos Trans. AGU*, *89*(53), Fall Meet. Suppl., Abstract S11D-05.

Sigloch, K., N. McQuarrie, and G. Nolet (2008), Two-stage subduction history under North America inferred from multiple-frequency tomography, *Nat. Geosci.*, *1*, 458–462, doi:10.1038/ngeo231.

Simmons, N., A. Forte, and S. Grand (2006), Constraining mantle flow with seismic and geodynamic data: A joint approach, *Earth Planet. Sci. Lett.*, *246*, 109–124, doi:10.1016/j.epsl.2006.04.003.

Steinberger, B. (2000), Slabs in the lower mantle-Results of dynamic modelling compared with tomographic images and the geoid, *Phys. Earth Planet. Inter.*, *118*, 241–257, doi:10.1016/S0031-9201(99)00172-7.

Tian, Y., R. Montelli, G. Nolet, and F. Dahlen (2007), Computing traveltime and amplitude sensitivity kernels in finite-frequency tomography, *J. Comp. Physiol.*, *226*, 2271–2288.

Tian, Y., K. Sigloch, and G. Nolet (2009), Multiple-frequency *SH* wave tomography of the western US upper mantle, *Geophys. J. Int.*, *178*, 1384–1402, doi:10.1111/j.1365-246X.2009.04225.x.

Tian, Y., Y. Zhou, K. Sigloch, G. Nolet, and G. Laske (2011), Structure of North American mantle constrained by simultaneous inversion of multiple-frequency *SH*, *SS*, and Love waves, *J. Geophys. Res.*, doi:10.1029/2010JB007704, in press.

van der Hilst, R., S. Widiyantoro, and E. Engdahl (1997), Evidence for deep mantle circulation from global tomography, *Nature*, *386*, 578–584.

van der Lee, S., and G. Nolet (1997), Upper mantle *S* velocity structure of North America, *J. Geophys. Res.*, *102*, 22,815–22,838.

van der Lee, S., K. Regenauer-Lieb, and D. A. Yuen (2008), The role of water in connecting past and future episodes of subduction, *Earth Planet. Sci. Lett.*, *273*, 15–27, doi:10.1016/j.epsl.2008.04.041.

van der Meer, D., W. Spakman, D. van Hinsbergen, M. Amaru, and T. Torsvik (2010), Towards absolute plate motions constrained by lower-mantle slab remnants, *Nat. Geosci.*, *3*, 36–40, doi:10.1038/ngeo708.

Virieux, J., and S. Operto (2009), An overview of full-waveform inversion in exploration geophysics, *Geophysics*, *74*, 127–152, doi:10.1190/1.3238367.

Wortel, M., and W. Spakman (2000), Subduction and slab detachment in the Mediterranean-Carpathian Region, *Science*, *290*(5498), 1910–1917, doi:10.1126/science.290.5498.1910.

Xue, M., and R. M. Allen (2010), Mantle structure beneath the western United States and its implications for convection processes, *J. Geophys. Res.*, *115*, B07303, doi:10.1029/2008JB006079.

Zhou, Y., G. Nolet, and F. Dahlen (2003), Surface sediment effects on teleseismic *P* wave amplitude, *J. Geophys. Res.*, *108*(B9), 2417, doi:10.1029/2002JB002331.

Zhou, Y., F. A. Dahlen, and G. Nolet (2004), 3-D sensitivity kernels for surface-wave observables, *Geophys. J. Int.*, *158*, 142–168.